Preface

The last step before graduating as Industrial Engineer in Electronics-ICT, is writing a master's thesis. After four years of study, we have been able to apply our theoretical knowledge into our 'own research'. We got the unique chance to learn a lot of new things during this master's thesis. On the one hand in the technical field, but on the other hand we got the opportunity to gain an initial experience in the medical world. The collaboration with Hartcentrum Hasselt and Jessa Hospital Hasselt, provided us the chance to exchange our technical expertise with the medical knowledge of the physicians.

The success of this research would not be possible without the support and experience of others. We like to thank our supervisors, our family and friends.

In particular, we want to thank our promotor, Dr. MD Pieter Koopman for his excellent guidance during the project. He gave us the chance to do this research but gave us also some other opportunities. We were allowed to attend a few surgeries in his CATHLAB. In September, we were invited to a symposium organized by Hartcentrum Hasselt 'Snapshots uit de Hasseltse ritmologie'. Last but not least, he presented our research during the BEHRA congress.

Prof. Dr. Ir. Luc Claesen was assigned by our faculty as internal promotor. We are thankful that he shared his knowledge and experience about image processing techniques with us. We could always count on him to give us useful feedback.

Finally, we like to thank Dr. Olivier Ghekiere, Dr. Eric Bijnens and Bram Van Elsen for helping us gather test data prepared in the most suitable conditions.

Table of Contents

List of Tables

List of Graphs

List of Figures

Glossary

TERM	DEFINITION
3D rotational angiography	a medical imaging technique to acquire a 3D model of the heart during the ablation procedure
ablation	a method to treat atrial fibrillation by deliberately corroding cardiac tissue with the help of radiofrequency, laser or cryothermal energy
atrial fibrillation	the most common cardiac arrhythmia caused by the movement of electrical signals in the heart in a completely disorganized manner
atrioventricular node	part of the electrical conduction system of the heart which connects the right atrium with the right ventricle
atrium	either of the two upper chambers on each side of the heart that receive blood from the veins and in turn force it into the ventricles
center of gravity	the point of a surface or volume to which the mass of that object is in balance
computed tomography	an imaging technique that uses radiant images to get more details of bone and tissue than on classic RX images
convolution	transformation of one function by another, the result is the area of the overlap of both function, with the second function shifting
cryoablation	an ablation technique that uses extreme cold to destroy tissue with the use of a fixed size balloon
depolarization	loss of the difference in charge
deuterium	an isotope of hydrogen, having twice the mass of ordinary hydrogen
diaphragm	the partition separating the thoracic cavity from the abdominal cavity
electrocardiogram	a recording of the electrical activity of the heart
endocardial pacing	electrical stimulation by using a pacing electrode
endoscopic	a slender, tubular optical instrument used as a viewing system for examining an inner part of the body
fibrous pericardium	the most superficial layer of the pericardium (a double-walled sac containing the heart and the roots of the great vessels)
gradient	the rate of variation of a numerical quantity
grey level image	an image where each pixel has a single value which represents its intensity
intra-esophageal probe	a probe that is placed in the esophagus to visualize it with rotational angiography during surgery and to check the temperature of the esophagus during ablation procedures
invasive	requiring the entry of a catheter into a part of the body
isotropic	uniform in all orientations
laser balloon ablation	an ablation technique that uses laser energy to destroy tissue with the use of an inflatable balloon
lateral side	the side of a body part that is the farthest away from the center of the body
low-pass filter	a filter that passes signals with a frequency lower than a certain cutoff frequency
mediastinal pleura	the outer portion of the membrane around the lungs, that separates them from and attaches them to the mediastinum
moving average filter	the average of a fixed number of consecutive elements of a dataset
ostium	a small opening
outlier	an observation that does not seem to fit the rest, usually a data point located far from the other points, outliers are often disregarded
pace mapping	a technique to locate tachycardia by stimulating certain regions of the heart to reproduce the tachycardia symptoms
palpitation	an unusually or abnormally rapid or violent beating of the heart.

pericardiacophrenic artery	branch of the internal thoracic artery, that is located adjacent to the phrenic nerve and runs between pleura and pericardium to the diaphragm, where it distributes the blood
phrenic nerve paralysis	damage of the PN resulting in prolonged breathing problems for the patient
pleura	membrane that is double-folded around each of the lungs forming a secretion between the lungs and the chest cavity
point-by-point RF ablation	an ablation technique that uses RF energy to destroy tissue with the help of a catheter
protocol	a predefined written procedural method
pulmonary hila	the part of the lungs located near the mediastinum, where the blood vessels enter and exit
pulmonary vein isolation	a treatment for atrial fibrillation by electrically isolating the pulmonary veins
quantized	a discrete value instead of a continuous one
sinus node	a group of cells in the heart that trigger the heart periodically to perform a contraction
structuring element	a shape used to interact with a given image to determine the pixel values of the output image
thoracic inlet	the opening at the top of the thoracic cavity
thresholding	a method for image segmentation by comparing pixels values to a constant
time complexity	the way an algorithm behaves as the size of the problem to be solved increases
tissue	a group of cells with a similar function
transverse aortic arch	the part of the aorta between the ascending and descending aorta
vena cava	the largest veins of the body, in which the blood flows together before it reaches the heart, the blood of the upper part of the body flows to the heart via the superior vena cava, the blood of the lower part of the body via the inferior vena cava
venous occlusion	when the blood flow through the vein is blocked
ventricle	either of the two lower chambers on each side of the heart that receive blood from the atria and in turn force it into the arteries
ventricular tachycardia	a cardiac arrhythmia in which the muscles of the ventricles contract irregularly in a rapid, uncoordinated manner, impairing the normal pumping of blood
wave fronts	a surface, real or imaginary, that is the locus of all adjacent points at which the phase of oscillation is the same

Glossary drawn up with the help of http://www.dictionary.com.

List of Abbreviations

ABBREVIATION	DEFINITION
AF	atrial fibrillation
RF	radio frequency
PN	phrenic nerve
CT	computed tomography
LA	left atrium
RA	right atrium
RANSAC	random sample consensus
DICOM	Digital Imaging and Communications in Medicine (file format standard)
ROI	region of interest

Abstract

In Hartcentrum Hasselt, patients with atrial fibrillation are treated invasively by performing pulmonary vein isolation. One of the techniques used for this procedure, is an endoscopic laser balloon ablation system. During this procedure, there is a slight risk of damaging the right phrenic nerve.

In this master's thesis, a method is developed to visualize the nerve before surgery on CT images. That way, the physician can assess the appropriate ablation areas and reduce the risk of phrenic nerve paralysis. During the previous bachelor's thesis, a 'proof of concept' showed that it is possible to identify the nerve by automatic nerve detection in a single patient. This master's thesis has the objective to improve and enhance the algorithm such that it is useful for a larger patient population.

The algorithm is designed in MATLAB. The processing of the images can be subdivided in four steps. After pre-processing the CT images to reduce the effect of unwanted noise, the various parts of the heart are segmented. By doing this, a small region of interest can be isolated where possible locations of the phrenic nerve can be identified. The last step is the 3D-reconstruction of the right phrenic nerve.

This thesis has led to a more robust algorithm that is able to determine the position of the nerve in 89 percent of the cases with a median error margin of 3.51 mm. However, when the CT slices are of inferior quality or when the contrast fluid is not clearly visible, problems can still arise.

Abstract in het Nederlands

In het Hartcentrum Hasselt worden patiënten met voorkamerfibrillatie invasief behandeld door pulmonaalvene isolatie. Eén van de mogelijke technieken hiervoor is ablatie met behulp van een endoscopisch laserballon ablatiesysteem. Bij deze ingreep bestaat het risico om de rechter nervus phrenicus te beschadigen.

In deze thesis wordt een methode ontwikkeld om de zenuw voor de ingreep te visualiseren op CT-beelden. Zo kan de arts de geschikte ablatiegebieden bepalen en het risico op een phrenicusparalyse beperken. In een voorgaande bachelorproef heeft een 'proof of concept' reeds aangetoond dat identificatie van de zenuw mogelijk is door automatische zenuwdetectie op één patiënt. Deze masterproef heeft als doel het algoritme te verbeteren en uit te breiden naar een grotere patiëntenpopulatie.

Het algoritme is ontworpen met MATLAB. De verwerking van de beelden gebeurt in vier stappen. Na voorverwerking van de CT-beelden om ruis te verminderen, worden de verschillende delen van het hart gesegmenteerd. Zo wordt een klein interessegebied afgebakend waarin op zoek wordt gegaan naar de mogelijke locaties van de zenuw. De laatste stap is de 3D-reconstructie van de rechter nervus phrenicus.

Deze thesis heeft geleid tot een robuuster algoritme dat in staat is om in 89 procent van de gevallen de positie van de zenuw te detecteren met 3,51 mm als mediaan van de afwijking. Wanneer de CT-scans echter van mindere kwaliteit zijn of de contrastvloeistof niet genoeg zichtbaar is, duiken er nog problemen op.

1 Introduction

1.1 Background

This research is commissioned by Hartcentrum Hasselt and Jessa Hospital, where patients with atrial fibrillation (AF) are treated. This AF is the most commonly encountered arrhythmia in clinical practice with a prevalence of up to 1 percent, causing a rapid and irregular heartbeat with symptoms of palpitations, shortness of breath or chest pains [1].

One of the common techniques to treat AF, is pulmonary vein isolation. There are several methods, such as point-by-point radiofrequency (RF) ablation, cryoablation and laser balloon ablation. This latter technique consists of inflating and positioning a small sized balloon at the ostium of the pulmonary veins. As venous occlusion is achieved by thorough tissue contact around the entrance of the pulmonary vein, energy can be delivered to the tissue to create a circumferential ablation lesion resulting in electrical pulmonary vein isolation. A potential risk during the pulmonary vein isolation is damage of the right phrenic nerve (PN) by involuntary heating [1].

During the procedure, the physician is guided by a model to navigate through the heart. This model is based on computed tomography (CT)-images made before the surgery or on a 3D rotational angiography made during the procedure. On these images, a 3D reconstruction of the contrast-filled left atrium (LA) and pulmonary veins is performed, which is used for guidance during the ablation procedure. The trachea and esophagus (by means of an intra-esophageal probe) can also be visualized.

1.2 Problem Definition

The model used during the procedure, does not show the location of the PN. Because of the potential risk of damaging the right PN during a laser balloon ablation, it is important that the physician can locate the nerve during the procedure. The risk is even higher when a cryoballoon is used, because of the fixed size of the balloon that could end deeper inside the pulmonary vein.

Currently the right PN is stimulated during the whole procedure resulting in a hiccupping patient. The hiccups should not disappear and this is constantly manually checked by a nurse by pressure on the diaphragm, as well as by measurement of the amplitude of the diaphragmatic electromyographic signal on the electrophysiology system. However, when a weakening of the hiccups is noticed, it is already too late and the nerve will be (partially) damaged. In that case, the procedure is stopped until the nerve recovers. In the worst case, the nerve remains damaged and the patient experiences prolonged breathing problems. This creates stressful working circumstances for the threating physician.

1.3 Objectives

The objective of this research is to visualize the location of the right PN on images of the heart before the procedure has started. This allows the physician to assess the appropriate ablation areas and areas of risk to avoid complications.

The research project can be divided in different stages. This master's thesis focuses on detection and reconstruction of the right PN on coronary CT scans. Further research can focus

on developing a similar algorithm for 3D rotational angiography, that has significantly lower resolution.

During the bachelor's thesis, a 'proof of concept' has showed that it is possible to identify the nerve by automatic detection on a single patient [1].

This master's thesis has the objective to improve and enhance the algorithm for a greater patient population by improving the pre-processing, the segmentation, the determination of the nerve area and the detection of the right PN. The final step is the reconstruction of the right PN on a 3D model of the heart.

The goal of this thesis is to develop an algorithm that is able to recognize the PN on a series of more than 15 patients and validate the results by pace mapping. Pace mapping is a process where the location of the PN is approximated by marking the zone where the nerve can be stimulated during endocardial pacing on its course on the lateral side of the superior caval vein and the right atrium.

1.4 Methods and Materials

To perform the image processing methods on the CT slices, the software MATLAB [2] is used because many image processing features are built in this mathematical package.

First the algorithm is designed for a small number of patients and then expanded to a larger population. After verification of the algorithm on the images of a large series of patients, the identified location will also be compared with the actual location of the nerve determined by pace mapping.

1.5 Outline

Chapter 2

This chapter focuses on the medical background of the underlying master's thesis. It contains information about atrial fibrillation, pulmonary vein isolation, ablation techniques and the phrenic nerves. Furthermore the location of the PNs is discussed. Even the currently used techniques for localization of the right PN, like pace mapping, are briefly reviewed.

Chapter 3

General information of the technical background of our project is given in chapter 3. The section gives a quick overview of the concepts of some functions that are used in the algorithm.

Chapter 4

Chapter 4 is the main part of this thesis. It contains all the information about the algorithm to detect and reconstruct the PN.

Chapter 5

In chapter 5, the results of the verification test from the algorithm are summarized. It gives an overview of the results of the new algorithm, developed in this thesis, on a group of test patients. The results are also validated by comparing them to the location of the nerve determined by pace mapping.

Chapter 6

This chapter discusses the results that are successful and the limitations of the algorithm.

Chapter 7
Finally, chapter 7 concludes what has been achieved during this master's thesis.

2 Medical Background

2.1 Atrial Fibrillation

Atrial fibrillation is the most common cardiac arrhythmia. This disorder causes a too slow or too fast, but always irregular heart rhythm. The heart consists of four chambers: two atria and two ventricles. Atrial fibrillation occurs when the atrial tissue does not contract simultaneously.

Normally, an electrical signal is created in the sinus node of the right atrium (RA), wherafter the signal spreads through both atria. This results in a depolarization through which both atria contract simultaneously. The electrical signal progresses through the atrioventricular node to the ventricles and stimulates them to contract.

In AF, electrical signals move in the atria in a completely disorganized manner, so the sinus node cannot send a clear signal anymore. Instead of one large contraction of the atria, the different muscle fibers will contract separately, resulting in very weak global contractile forces and absence of a clear atrial contraction.

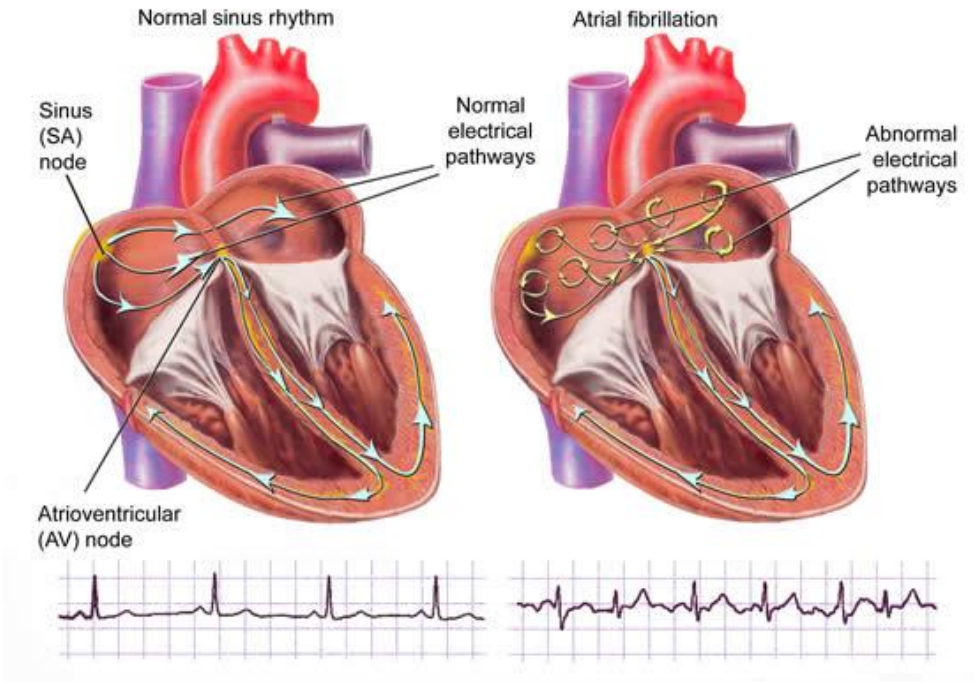

Figure 1: Normal sinus rhythm vs atrial fibrillation [3]

AF can also be derived from the electrocardiogram. Normally there is a clear P-wave which indicates the contraction of the atria, as shown in Figure 2. This wave is followed by a large peak, the QRS-complex, also known as the signal of the contraction of the ventricles.

Patients with AF have several small peaks on their electrocardiogram before the QRS-complex. These show that there are several weak contractions of the muscle fibers of the atria. The electrical signal reaches at some times enough strength to progress to the ventricles and produce a QRS complex, that are appearing irregularly.

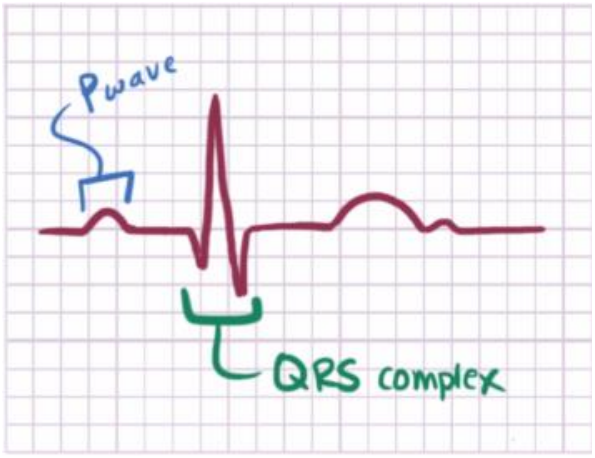

Figure 2: Normal electrocardiogram [4]

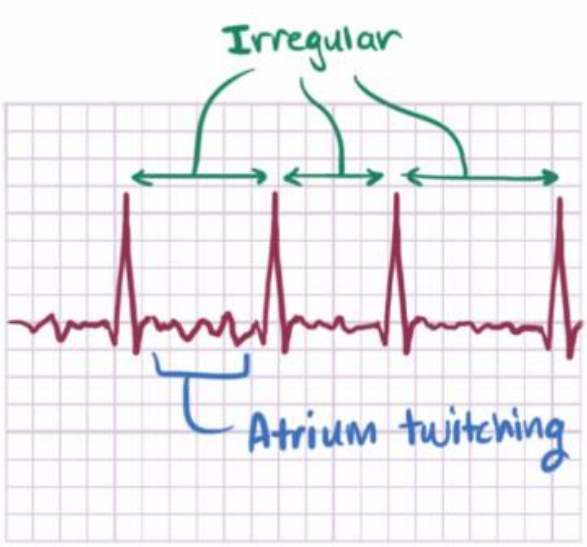

Figure 3: Electrocardiogram with atrial fibrillation [4]

A possible trigger of AF is atrial ectopy, an electrical signal that originates from a different location in the heart and earlier than the signal of the sinus node. These ectopic signals can disrupt the normal electrical activity of the heart, resulting in the fast disorderly wave fronts of AF. Often these signals arise in the disarrayed muscle fibers inside the pulmonary veins. This can be treated by pulmonary vein isolation [4].

2.2 Pulmonary Vein Isolation

Because the electrical signals that disrupt the contraction of the atria are frequently formed in the pulmonary veins, electrical isolation of them can resolve the problem.

The pulmonary veins enter the heart at the posterior wall of the LA. With the help of various ablation procedures, it can be ensured that the electrical signals that originate from these veins are no longer able to reach the heart.

There are different types of ablation procedures. Point-by-point radiofrequency ablation catheters or different types of balloon catheters (cryoballoon or laser balloon) can be used. An advantage of the balloon catheter is that the ablation procedure takes less time. A balloon can ablate a large area simultaneously, while a radiofrequency catheter must treat the tissue point-by-point. Therefore, in most of the cases, balloon catheters are used for pulmonary vein isolation [5]. During ablation, the balloon is located into the pulmonary vein ostium where the latter connects to the LA. Subsequently, the balloon is inflated and the heart tissue is ablated at the contact site, using cryo or laser energy, right at the transition of the LA and the pulmonary vein.

The cryoballoon (Figure 4) uses nitrous oxide (laughing gas) to ablate the tissue by freezing. A cryoballoon has a fixed size because it should always be fully inflated. Because the size of the veins may widely vary among different patients, the balloon sometimes moves deeper into the pulmonary veins than desired or in other cases, cannot even pass the opening to the pulmonary veins. Hence the physician cannot always choose the ideal ablation position which increases the risk of paralyzing the right PN.

A major advantage of the laser balloon (Figure 4) is its variable size that can be adapted to the anatomy of the patient. The balloon also features a miniature endoscopic camera, an optical fiber for the delivering of laser energy and a narrow tube that circulates deuterium (heavy hydrogen) to fill the balloon and allow for good visualization through the endoscopic camera [5].

Figure 4: Balloons for ablation procedures; left: cryoballoon, right: laser balloon

In most hospitals, a cryoballoon is used to perform the ablation. However the Jessa Hospital in Hasselt, as the only center in Belgium, has adopted the newer laser balloon technique.

2.3 The Phrenic Nerves

The phrenic nerves are nerves that have an important function for respiration. They are responsible for the transport of a stimulus from the brains to the diaphragm. Damage of the PNs results in paralysis of the diaphragm that consequently does not move downward anymore during inhalation. This results in a smaller lung capacity and as such decreases the respiratory efficiency.

During the execution of an ablation in the LA, there is a potential risk of damaging the right PN. Both balloon techniques have a higher risk of PN damage, because ablation with the balloon technique occurs closer to the ostium of the pulmonary veins (or even inside the veins) than radiofrequency ablation. Studies have shown that the risk of phrenic nerve paralysis is 8 percent for ablations with a cryoballoon [6] and 2,5 percent using the laser balloon technique [7]. Damage may occur due to overheating of the nerve by the energy used during the ablation. Damage of the nerve may result in short-term, long-term or even permanent failure of the nerve, together with the associated respiratory problems [8].

The left PN cannot be damaged by performing pulmonary vein isolation for atrial fibrillation, but could be damaged during other types of ablation procedures, such as ablation of ventricular tachycardia in the left ventricle.

2.3.1 Location

The PNs are located in the chest between both lungs and the heart, and run their course from the thoracic inlet down to the diaphragm. The nerves are situated in the middle of the pleura and the apex of the right or left lung.

The right phrenic nerve is located lateral to the right atrium and the superior vena cava. The left phrenic nerve runs along the lateral part of the transverse aortic arch. The phrenic nerves

run anteriorly to the pulmonary hila and then go inferior in a wide vertical plane along the edge of the heart between the fibrous pericardium and mediastinal pleura [9].

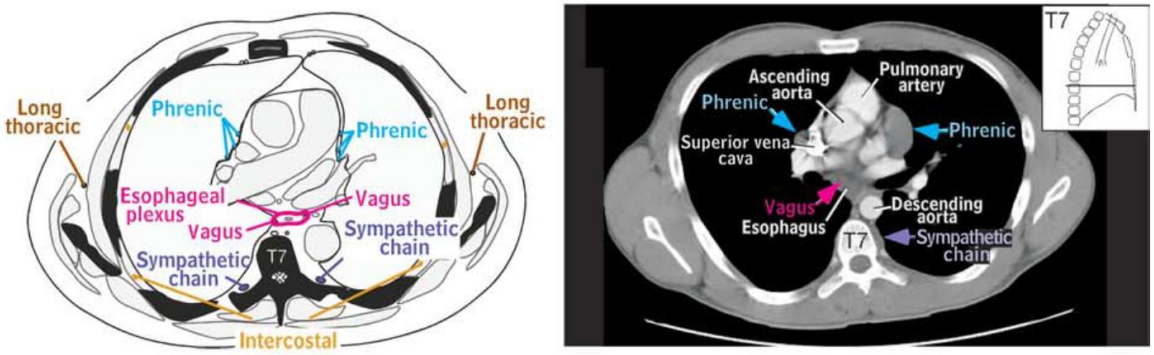

Figure 5: Schematic drawing of the location of the PN + PN located on an axial CT scan [9]

2.3.2 Localization Techniques

Pace mapping

Currently the right PN can be detected by pace mapping. A mapping catheter is used to assess the anatomic location of the nerve. Pacing is performed and PN capture is defined as a fluoroscopically visible or palpable movement of the right diaphragm. These capture points can be indicated by means of specific mapping software with different colors according to the kind of response [10].

CT scans

The right PN cannot be easily detected on coronary CT scans because there is no difference between the radiographic tissue density of the right PN and the densities from surrounding structures. On the other hand, the right PN travels parallel to the right pericardiacophrenic artery and vein. Therefore, detection of these veins is sufficient to determine the right PN location. This is proven in the study by Horton et al. [11]. In his research, CT's with a late imaging protocol (venous phase) are used and segmentation is performed manually.

3 Technical Background

The book 'Digital Image Processing using MATLAB' [12], is a standard university course text. It introduces various types of image processing techniques. In this chapter a short overview of the techniques that are used to detect the PN, is given.

3.1 Image Processing

Image processing is a technique that uses mathematical operations to transform an input image to an output image. An image is a two-dimensional function. This function has an x and y argument that corresponds to the location of a pixel in the image. For every value of x and y, the function value $f(x, y)$ represents the intensity of the pixel. In this thesis, the pictures are digital images. That means that the amplitude of each pixel is quantized.

3.2 Intensity Transformation and Spatial Filtering

Intensity transformation and spatial filtering can be defined by the following equation:

$$g(x, y) = T[f(x, y)]$$

Equation 1: Image transformation

$f(x, y)$ represents the original image and $g(x, y)$ is the result of the transformation T. In case of an intensity transformation, the transformation is applied on every single pixel of the image. Spatial filtering uses a small region of pixels of the image. On these pixels the transformation T is applied.

3.2.1 Intensity Transformation

A simple intensity transformation uses the operator T, an intensity transformation function, which is applied on every pixel of the image. Figure 6 shows an example of an intensity transformation, namely the gamma transformation, with on the x-axis the intensity levels of the input image and on the y-axis the intensity levels of the output images. The graph with a gamma lower than 1 makes the picture darker and a gamma higher than 1 results in a brighter picture. This can also be derived from the formula:

$$g(x, y) = f(x, y)^{\gamma}$$

Equation 2: Gamma transformation

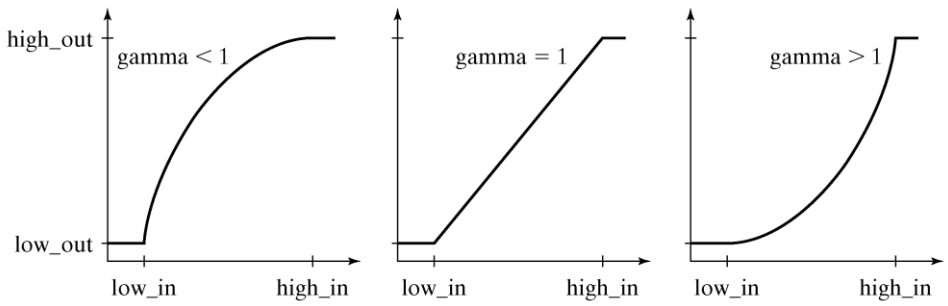

Figure 6: Gamma-correction [12]

3.2.2 Spatial Filtering

Spatial filtering performs mathematical operations on a group of pixels within a certain area and replaces the middlemost pixel with the outcome of this operation. In contrast to intensity transformation, spatial filtering carries out calculations on several neighboring pixels. This filtering method is used to remove unwanted noise, while keeping edges and transitions intact.

First of all, the filter chooses an area around a central pixel. On these pixels a transformation is applied. Then the central pixel of the area is replaced by the result. Afterwards the central pixel is shifted. These steps are iterated for the whole image. Figure 7 shows an example of such an area with the central pixel indicated.

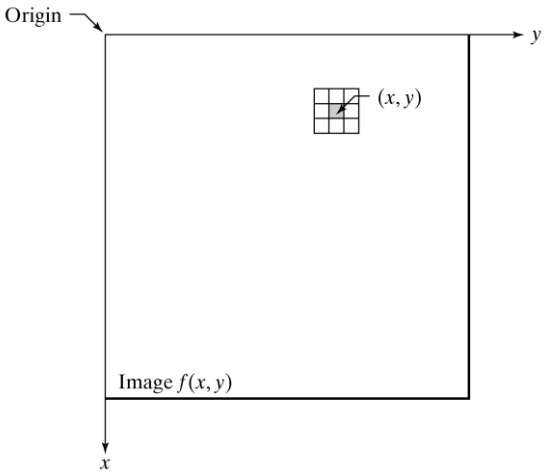

Figure 7: Spatial filtering [12]

There are two kinds of spatial filters: linear and non-linear filters. An example of a linear spatial filter is a 3x3 averaging filter. The transformation is a convolution of the area of neighboring pixels with the mask described in Equation 3. This filter will blur and reduce the noise in an image.

$$\frac{1}{9} * \begin{bmatrix} 1 & 1 & 1 \\ 1 & 1 & 1 \\ 1 & 1 & 1 \end{bmatrix}$$

Equation 3: Average spatial filter

The second kind of spatial filters is a non-linear filter. This filter uses non-linear transformations. An example is a median filter. This filter calculates the median value of the pixels within a certain area, and replaces the middlemost pixel with this median value. Figure 8 shows a case how a median spatial filter works. The intensity values within the mask are ranked from low to high. The median of these pixels is equal to the middlemost number. The central pixel of the mask is then replaced by the median.

20	35	23	21	40
60	63	54	58	69
34	55	35	37	46
56	65	74	34	32
54	55	45	65	66

34 – 35 – 37 – 54 – 55 – 58 – 63 – 65 – 74

Median value: 55

Figure 8: Median spatial filter

3.3 Image segmentation

Image segmentation is an important topic in this thesis. Segmentation allows to subdivide an image in meaningful regions. A region can be characterized by its properties like: grey level, texture, color etc. There are several methods to extract such an area. Edge detection (edge-based segmentation) and thresholding (region-based segmentation) are commonly used techniques.

3.3.1 Edge-based segmentation

An edge in an image is an abrupt change in intensity level. This change can be located by calculating the first and the second derivate. There are several ways to detect edges, for instance Sobel, OSTU Algorithm, Prewitt, Canny, … The technique used in this thesis is the Canny edge detector [13]. It is one of the most commonly used edge detectors.

The operation of the Canny edge detector can be explained in four steps. The first step is filtering the image with a low-pass filter for smoothing. By doing this, the noise in the image is reduced. The next step is calculating the gradient and the edge direction in every point. An edge point can be defined where the gradient and the edge direction are the strongest. The third step is eliminating edge points by comparing them with a threshold. In this way, the weak edge points are deleted. The last step is connecting all the edge points that are eight-connected into a boundary. Eight-connected means that two pixels touch each other at one of the eight neighboring places (horizontally, vertically or diagonally).

3.3.2 Region-based segmentation

Extracting a region from an image is done by thresholding. This is a technique to detect surfaces with the similar intensity levels. Equation 4 defines the principle of thresholding.

$$g(x,y) = \begin{cases} 1 & if\ f(x,y) \geq T \\ 0 & if\ f(x,y) < T \end{cases}$$

Equation 4: Thresholding formula

Any point with an intensity level above the threshold is called an object point. Otherwise, the point is called a background point. To choose the appropriate threshold, there are several

methods. A global threshold defines the same limit for the entire picture, while local thresholding varies along the figure and is useful for images with unequal background illumination.

The image can even be split up in more than two intensity levels. To accomplish this, more than one threshold value is selected. In this manner, a specific interval of intensities can be extracted from the figure.

In this thesis global thresholds are determined by automatic visual inspection of the image histogram. The peaks in the histogram are used to define the boundary values. This is further explained in the section 'Detection and reconstruction of the right Phrenic Nerve'.

3.4 Morphological Image Processing

The identification of objects in images is not an easy task. One way to simplify this is by converting a grayscale or colored image into a binary picture. Instead of a large amount of pixel intensity values, a binary image has only two possible values for each pixel: 0 or 1. This makes it possible to detect morphological structures. The original image is converted to a binary one by thresholding the original intensity values, as explained in the previous chapter.

Sometimes, the obtained image has to be enhanced by removing tiny structures or filling up holes. There are several techniques to accomplish this. Commonly used methods are erosion, dilation, opening and closing. All those methods are based on set theory.

3.4.1 Erosion

Erosion is an operation to thin objects in a binary image. It uses a structuring element B, which can have several shapes like a rectangle or a circle. The first step is moving the structuring element over the binary image. At each location, it is verified if the structuring element completely fits into the white parts of the binary image. If this is the case, the central pixel gets pixel value 1 in the resulting image. If not, the central pixel becomes black in the new picture.

The mathematical representation of erosion is: $A - B = \{z \mid (B)_z \subseteq A\}$ with original image A and structuring element B.

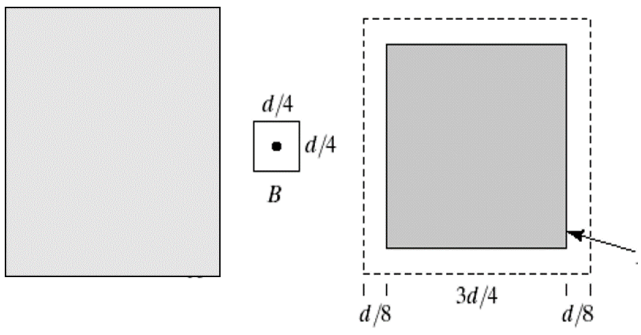

Figure 9: Erosion [12]

3.4.2 Dilation

Dilation is an operation to thicken objects in a binary image. The method is similar to erosion. The difference is that not all the pixels under the structuring element have to be white to get

a pixel value 1 in the output image. Only one pixel is sufficient. By doing this, the original image grows because several pixels that were originally black, are now converted to white pixels.

The mathematical representation of dilation is: $A \oplus B = \left\{ z \mid \left(\hat{B} \right)_z \cap A \neq \phi \right\}$ with original image A and structuring element B.

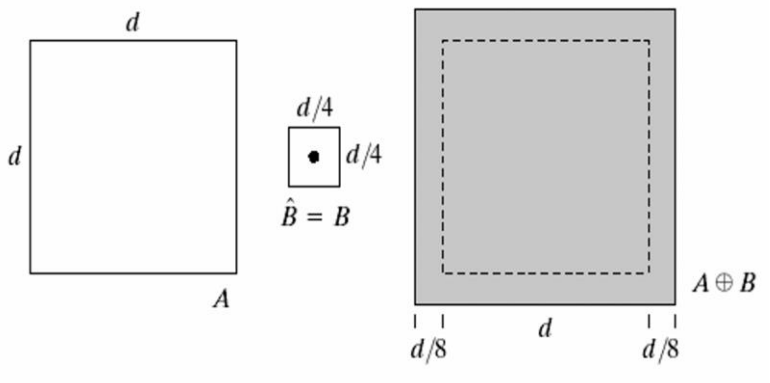

Figure 10: Dilation [12]

3.4.3 Opening and closing

Opening and closing are combinations of erosion and dilation. Opening is defined as an erosion operation followed by a dilation operation. The opening takes care of sharp edges and breaks thin connections. Besides it eliminates small islands and smooths the boundaries of the binary objects. Closing is the opposite of opening. First a dilation operation is applied on the image and after that an erosion operation. Closing smooths the image, fills holes in objects and fuses narrow breaks. Figure 11 and Figure 12 are representation of both methods.

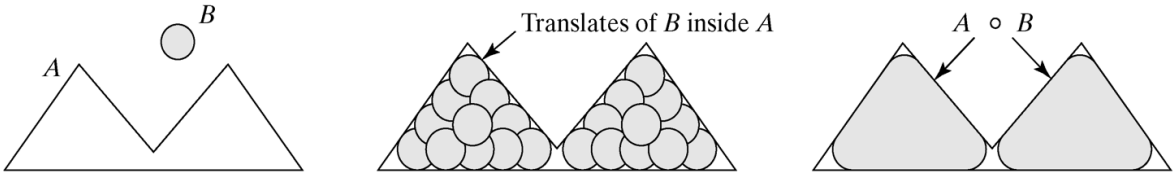

Figure 11: Opening [12]

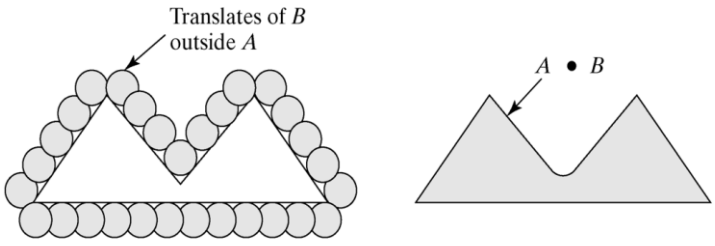

Figure 12: Closing [12]

3.5 Random sample consensus

Random sample consensus (RANSAC) [14][15] is a mathematical model for determining shapes by randomly selecting the minimum amount of points and constructing a primitive shape. The minimum amount of points is the smallest number of candidates that are required to reconstruct a primitive geometric shape in a unique manner. Afterwards, this primitive shape is tested to the whole dataset by counting the inliers, this results in a score. After a number of iterations, the shapes with the highest scores (the most inliers) are retained. These are good approximations of the geometric shapes that exist in the data cloud. One of the advantages of using RANSAC is that outliers are not taken into account, in contrast to the classical techniques for parameter estimation such as the least squares method. RANSAC is also conceptually easy to understand which makes it simple to implement.

The RANSAC method can be described as follows: First 2 points are randomly selected in the 3D data cloud. Afterwards a line is formed by connecting these 2 points. A point of the data cloud is an inlier when it falls within a perimeter around the reconstructed line. The perimeter can be specified by an input parameter. This procedure iterates for a given amount of times. As a result, lines are constructed in the 3D data cloud. If a constructed line counts a lot of inliers, the approximation will be more accurate [14], [15]. Inspired by the principle of RANSAC, a new algorithm to detect and reconstruct a straight line in a 3D data cloud, is developed in this thesis.

4 Detection and reconstruction of the right Phrenic Nerve

The algorithm to detect and reconstruct the right PN can be subdivided in four steps. The first thing to do is pre-processing the CT images to reduce the effect of unwanted noise. The second phase is the segmentation of the heart image to determine a small area where the right PN can be found. After that, possible locations of the right PN are detected in each CT slice by searching for the regional maxima in the nerve area. Finally, the right PN is reconstructed by looking for the best fitting curve in the 3D data points of possible PN locations.

4.1 Image pre-processing

The first thing to do is loading the DICOM (Digital Imaging and Communications in Medicine) [16] images from the patient into the MATLAB software. Each CT scan consists of a series of CT slices, each of them is saved in a DICOM image file. DICOM images consist of a header, followed by the data for the pixel intensities. The header file stores information about the patient as well as information about the image itself. Using the header information, the image can be reconstructed [17].

To process the images in MATLAB, there is a need for grayscale images because the algorithm is based on visual aspects of the CT slices. Therefore the MATLAB function *dicomread()* is used [18]. To enhance the image, the range of intensities has to be adjusted to a subset. This is done by dropping meaningless pixel values. To accomplish this, the header information is used to determine the meaningful window, specified by its size and center value [19].

The formula to acquire the correct greyscale image with window center value c and window width w is:

$$imgScaled = 255 \cdot \frac{((double(img) - (c - 0.5))}{(w - 1)} + 0.5$$

Equation 5: Conversion to greyscale image

After that, the meaningless pixel values outside the interval are set to the minimum (0) and maximum (255) value. Figure 13 shows the usefulness of this conversion.

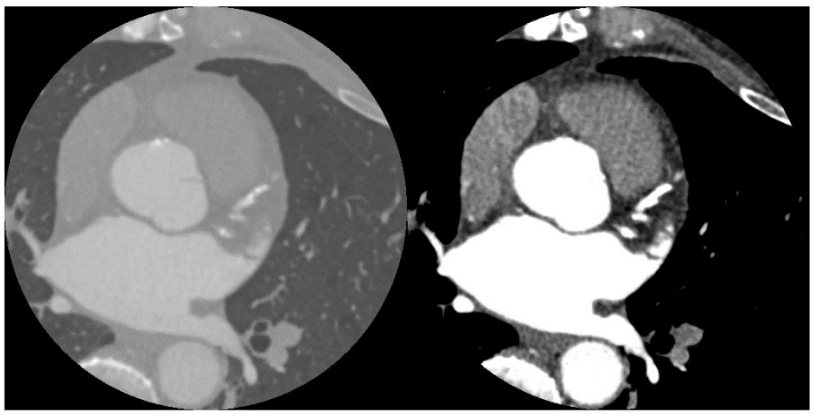

Figure 13: Comparison between unprocessed and processed DICOM-image

The next step is denoising the image to facilitate the segmentation step. This is done by applying a linear inhomogeneous isotropic filter, developed by Ritwik Kumar [20]. This filter removes unwanted noise while preserving the edges, illustrated in Figure 14.

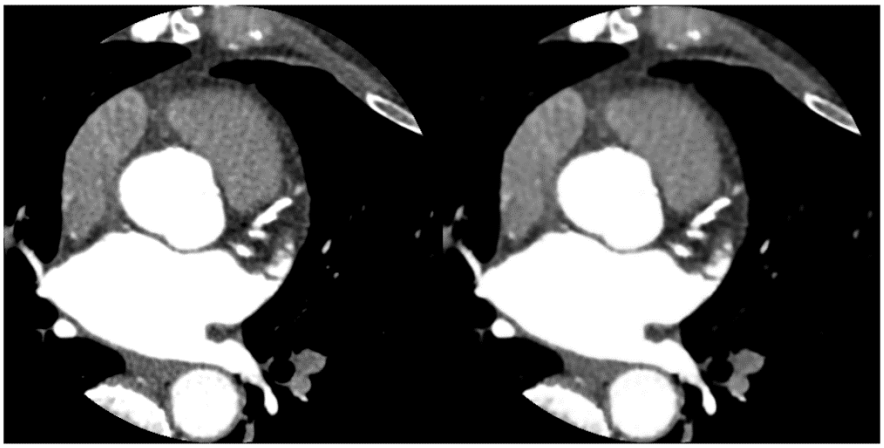

Figure 14: CT slice before and after applying the linear inhomogeneous isotropic filter

4.2 Segmentation

The segmentation of the CT slices is done in four steps. First of all, the contrast fluid areas are detected. These areas have a higher and brighter intensity than the other parts of the heart. By doing this, the LA and aorta can be separated. In a second step, the outer boundary is determined. The third step is the segmentation of the RA and right ventricle. These regions have a grey intensity, so they are brighter than the surrounding parts but darker than the areas with contrast fluid. The last step is the determination of the nerve area. This is a small region with possible locations of the PN. The area can be determined by combining the information obtained during the previous segmentation steps.

4.2.1 Segmentation of the Contrast Fluid

The segmentation of the contrast fluid starts with the construction of the image histogram. A histogram is the representation of occurrence frequency of intensity values in a picture. When represented as a bar graph, each bar of the graph represents the amount of pixels with a certain grey level interval, corresponding to the width of the bar. The peaks in the histogram correspond to large amounts of pixels with the same intensity. Usually these pixels are grouped in the image. These groups with similar intensities correspond to structures of the heart. By thresholding the images, these structures can be isolated. The shape of the histogram is a useful basis for the determination of specific threshold values.

The contrast fluid is visualized as an area with a high intensity. The high intensities are situated at the right side of the histogram. This means that a high peak will occur in this region. This peak can be separated by finding the appropriate threshold. To do this, a curve is fitted over the data in the histogram. To reduce the impact of noise, the curve is smoothed with a moving average filter. A peak is a sequence of a minimum, a maximum and another minimum. Because the peak is situated near the end of the histogram, the last but one minimum forms the threshold value. To detect the peaks of the smoothed curve, the algorithm of Eli Billauer is used [21]. Figure 15 shows the histogram of the CT slice with the chosen threshold indicated. Figure 16 is the resulting image of this segmentation.

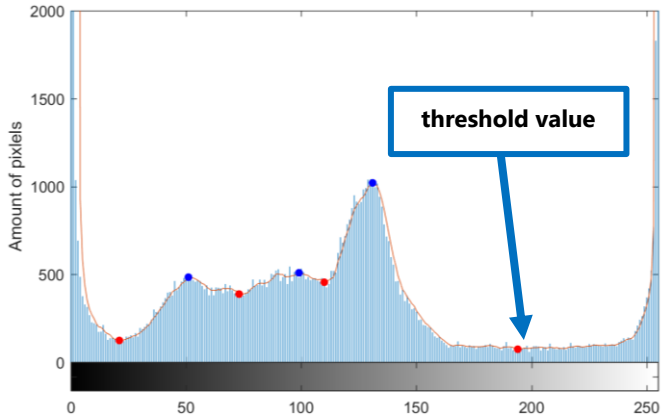

Figure 15: Histogram CT slice

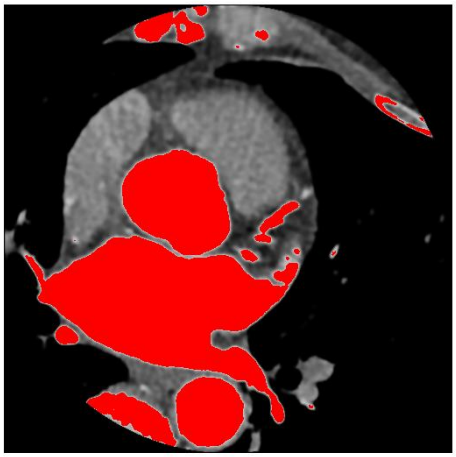

Figure 16: Segmentation of the white contrast

Sometimes when the contrast fluid does not have a uniform intensity, there are little unwanted peaks at the end of the histogram (Figure 17). In this case, not all the contrast fluid is segmented. Therefore the threshold has to move to the left until all the parts with contrast fluid are segmented. It has been determined by trial-and-error that at least 6 percent of the total number of pixels in the image has to be detected as white contrast. If not, the threshold value is shifted one minimum to the left. Figure 18 shows an example when the contrast fluid is not fully segmented and when the threshold is shifted.

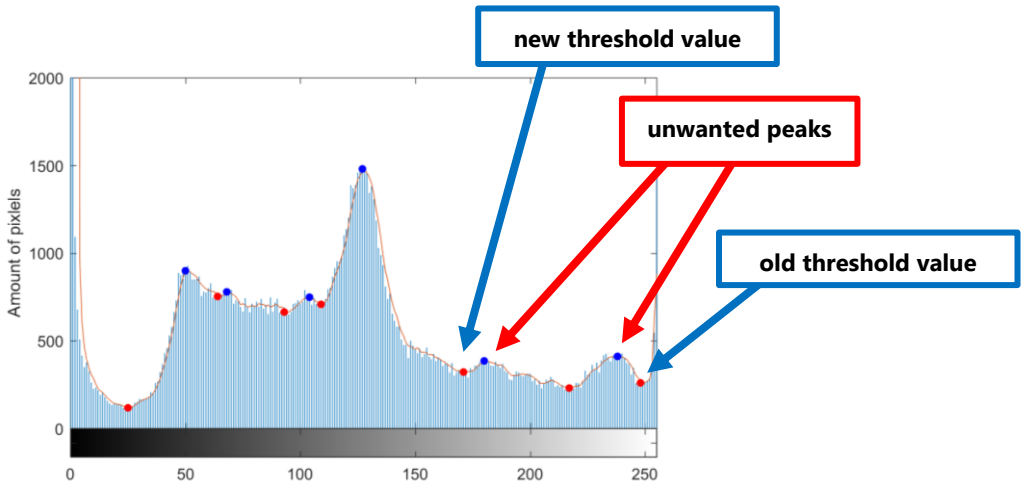

Figure 17: Histogram with unwanted peak at the end

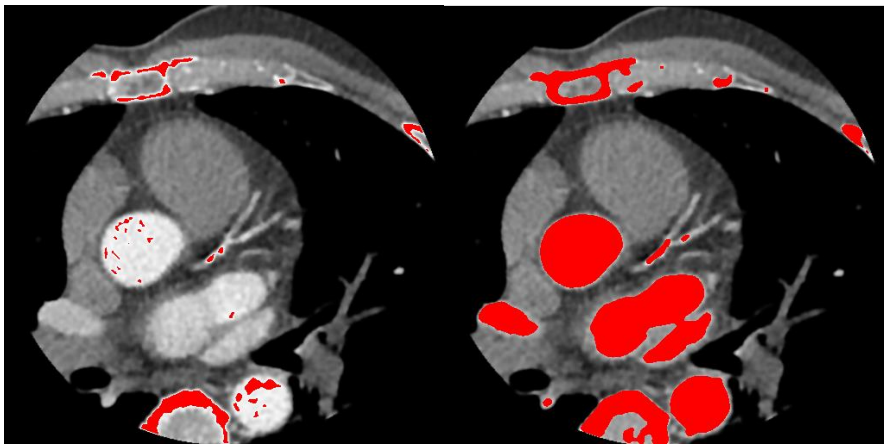

Figure 18: The white contrast before and after shifting the threshold value

Furthermore, the amount of pixels with white contrast cannot vary a lot between two sequential CT slices. An additional verification step is the comparison of the detected area between the slices. If the result varies a lot, it can be assumed that the chosen threshold is not the appropriate one. In that case, the threshold is adjusted to the previous minimum.

The segmented parts of the heart with white contrast contain the aorta and LA but also some less interesting regions. To extract those important pieces of the hearth, the two greatest areas can be selected. But in some cases, the aorta and LA are connected. In that case, only the greatest surface is extracted. Figure 19 shows the result of this segmentation.

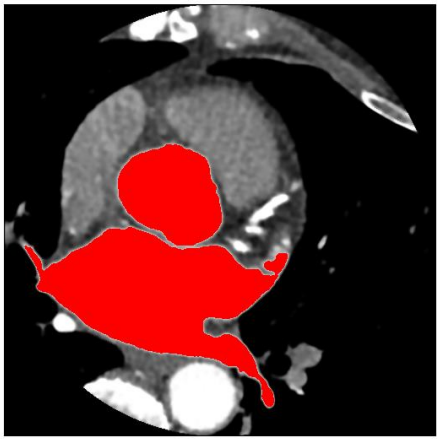

Figure 19: Segmentation of the aorta and LA

4.2.2 Cardiac Edge Detection

The cardiac edges are the outer boundaries of the heart together with the boundaries around the contrast fluid areas. These are required to detect the nerve area. They can be determined by removing the contrast fluid regions and the background from the CT slice.

The contrast fluid can be removed by taking the complement of the binary image of the contrast fluid. This results in an image (Figure 20) where all the pixels, except the ones with contrast fluid, have pixel value 1.

Figure 20: Complement of the binary image of the contrast fluid

The background can be removed by thresholding the original image. The threshold value is the first minimum of the histogram. Small impurities with an intensity slightly higher than 0 are

removed in this way. In the remaining picture (Figure 21), only the pixels that are member of the hearth have pixel value 1.

Figure 21: Elimination of the background

By combining the two previous pictures, the desired image can be found (Figure 22). This image consists of the parts of the heart with an intensity between the black background and the white areas with contrast fluid. By using the methods, discussed in section 'Morphological Image Processing', small islands and small holes are removed. The boundaries of these regions correspond to the cardiac edges (Figure 23).

Figure 22: Heart without background and white contrast

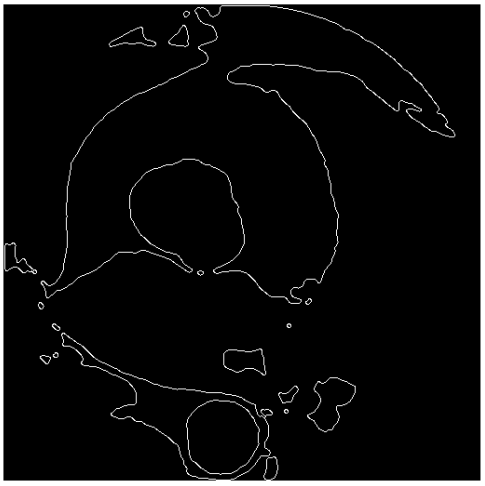

Figure 23: Cardiac edges

4.2.3 Segmentation of the Right Atrium and Right Ventricle

To detect the right atrium and right ventricle, a region of interest (ROI) is defined. By minimizing the size of the area, the proportion of grey colored pixels increases, what makes them easier to detect. Therefore the first step is selecting a region that contains the right atrium. The boundaries of this region are based on the previously segmented aorta and LA.

Because, the right atrium is situated at the left side of the images, the white contrast at the right side of the figure is not taken into account. The upper limit of the ROI is defined by the top point of the aorta (= anterior). The x-coordinate of this point also forms the right boundary for the ROI. The lower limit of the ROI is equal to the lowest point of the LA at this coordinate.

Finally, the left border is determined by the external boundary of the heart. Figure 24 indicates the selected ROI.

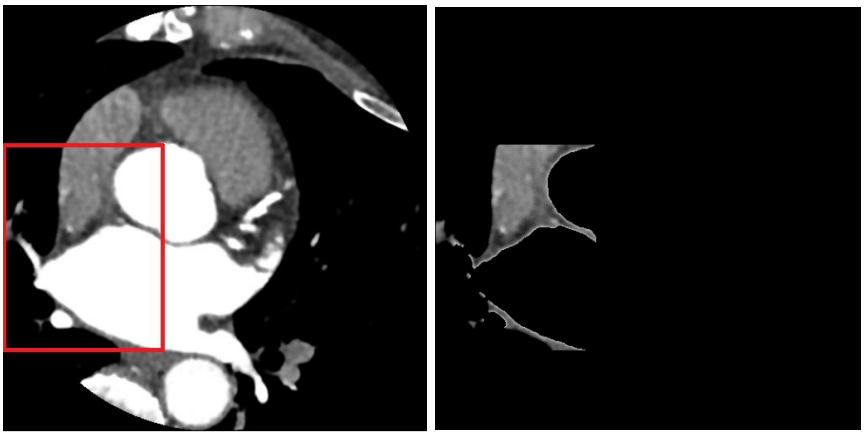

Figure 24: ROI for RA-detection

After the determination of the ROI, this area is smoothed by applying a median filter (Figure 25). Because there is no large variation in intensity levels, a subset of the histogram is selected and the contrast of this set is stretched. This is done by performing a transformation from the input pixels and mapping them to a new output level. Figure 26 shows the histogram of the ROI. The purpose is to spread the intensities between the first and last maximum over an intensity interval which is twice as wide as in the original image. Figure 27 is the graphical representation of this mapping procedure. By applying this transformation, the contrast of the image is enhanced, this is shown in Figure 29.

Figure 25: Median filtering of ROI for RA-detection

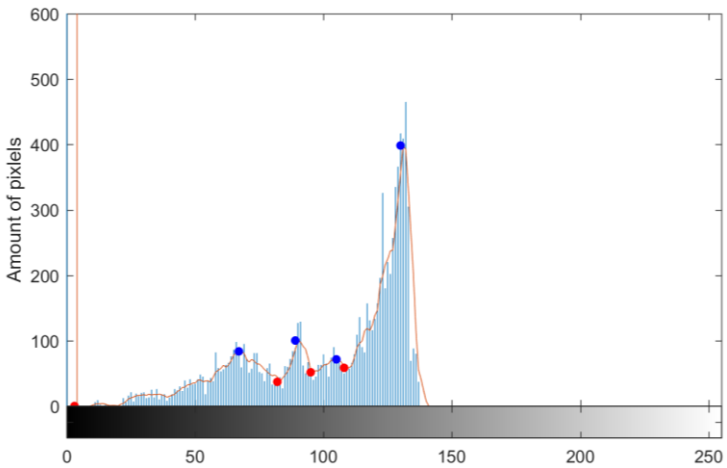

Figure 26: Histogram ROI for RA-detection

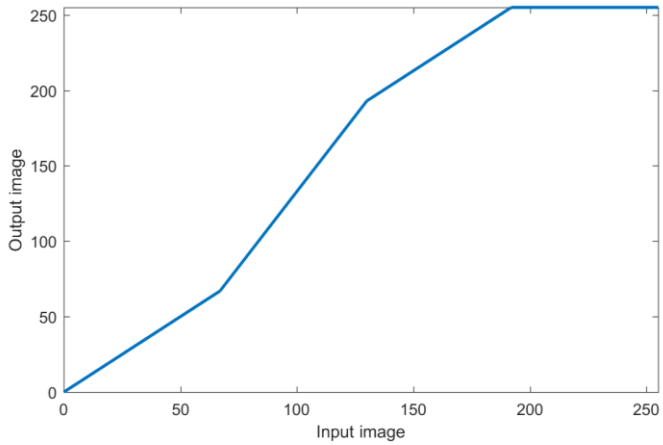

Figure 27: Contrast stretching equation

Figure 28: ROI after contrast stretching

The next step is multi-threshing this ROI. This means that the region is subdivided in multiple parts with different contrast by thresholding the figure with multiple thresholding values. The thresholding values can be automatically determined by MATLAB by choosing the number of desired contrast levels. In this case, the ROI is divided in three different areas. After that, the RA is segmented by selecting from these the region with the highest contrast. The selected area is indicated in Figure 29. When the threshold value of the previous step is applied on the whole image, the location of both the RA and the right ventricle can be determined. Figure 30 shows the result.

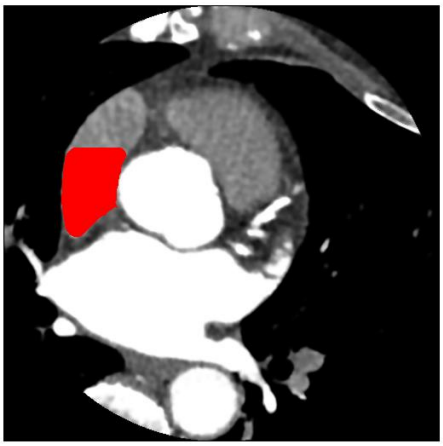

Figure 29: Detection of the RA in the ROI

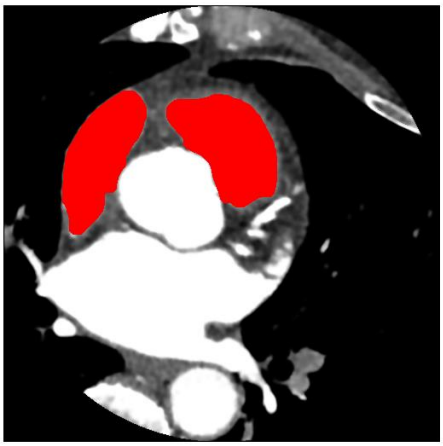

Figure 30: Segmentation of the RA and right ventricle

In some cases, the ROI contains other areas with the same intensity, which are not part of the RA. To avoid segmenting these regions, the detected RAs of all the CT slices are summed op. Then a mask is defined, which contains the pixels that are indicated as RA on at least 50 percent of the CT slices. After that, the detected RA on each slide is split up in objects from connected pixels. The RA is formed by the objects that overlap with the mask.

4.2.4 Determination of the Nerve Area

The nerve area can be found by subtracting the RA from the ROI determined in the previous section (Figure 31). To facilitate the detection of the nerve, the region is minimized by defining other rules for the upper, lower and right bound. The upper bound of the area is defined by the middle point of the RA. The lower bound is formed by the center of gravity of the LA when the aorta and LA are not connected with each other. Lastly the right bound is set by the x-coordinate of the lowest point of the RA. The result is shown in Figure 32. Another condition is that the nerve area has to touch the RA, therefore the areas that do not, are removed from the nerve area. The final reduced nerve area is indicated in Figure 33.

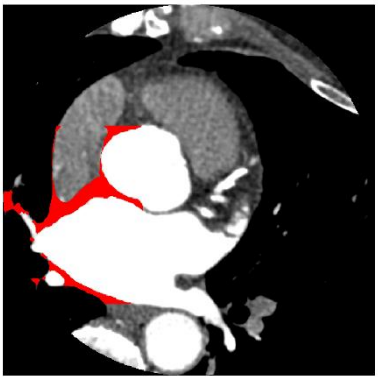

Figure 31: Determination of the nerve area - step 1

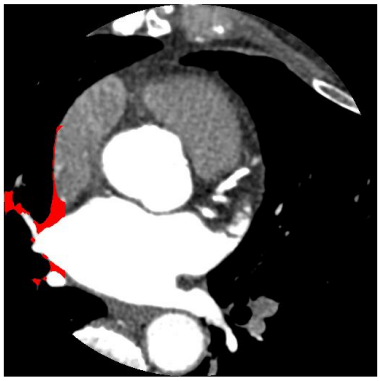

Figure 32: Determination of the nerve area - step 2

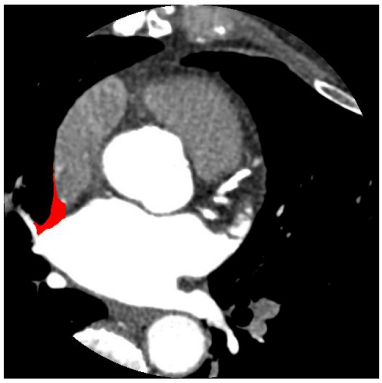

Figure 33: Determination of the nerve area - step 3

4.3 Detection of the Phrenic Nerve

The right PN is located in the isolated nerve area and as mentioned in '2.3.2 Localization techniques', the right PN can be recognized by a dot of higher intensity and surrounded with darker intensity pixels. These points can be found by searching for regional maxima. In the nerve area, there are a lot of candidate points and one of them may correspond to the right PN. The other points are derived from other structures, such as veins and noise. The detected points on one slice are indicated in Figure 34. A lot of noise points arise at the boundaries of the white contrast and the RA. To decrease the number of points, the detected dots that are too close to these edges are removed. The remaining possible nerve locations are shown in Figure 35.

Comparison of the PN location on the CT slices of various patients has shown that the nerve is located near the outer boundary of the heart. Therefore only the dots that are not too far away from this edge are used in the next step.

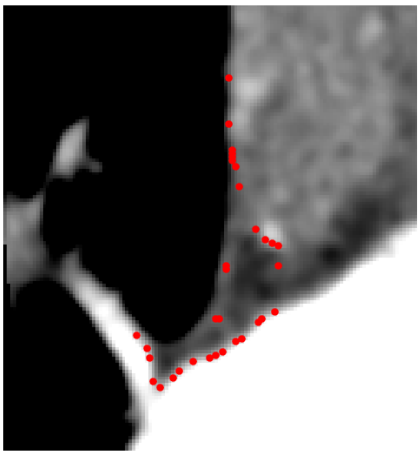

Figure 34: Regional maxima

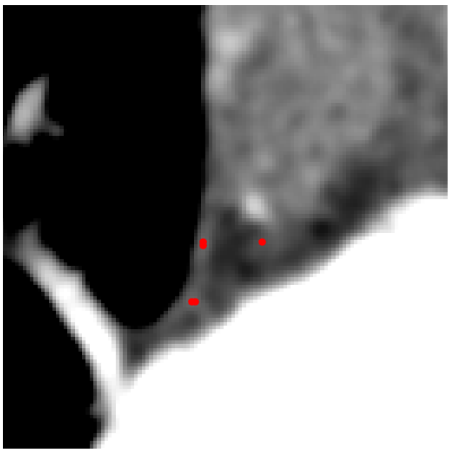

Figure 35: Possible PN locations

On some slices the appropriate location cannot be found by a regional maximum. Therefore it is necessary to combine the candidate points of all the slices in a 3D point cloud to search for the nerve location, this method is described in the next section 'Reconstruction of the Phrenic Nerve'.

4.4 Reconstruction of the Phrenic Nerve

The PN is located in the detected 3D point cloud. To determine the actual location of the PN, the best fitting line in this cloud is identified. To accomplish this, a variant of the RANSAC method, the "PN reconstruction algorithm", is developed. Instead of randomly choosing points of the point cloud to generate a line, all the possible lines formed by the regional maxima of the 10 highest CT slices with the regional maxima of the 10 lowest CT slices are determined. A line that connects a point in one of the highest slices with a point of one of the lowest slices has to be found, because the general path of the right PN forms a straight line which travels through all the CT slices in the selected range. It is important that all the possible combinations are checked and not only some random pairs to get always the same result. Attachment A shows the pseudo code of the PN reconstruction algorithm.

The best fitting line can be identified by counting the number of inliers. Then the ratio of each line is computed by dividing the number of inliers by the length of the line. The line with the highest ratio is chosen as the one that represents the location of the PN.

To better approach the actual location of the nerve, on each slice the regional maximum which is located the closest to the selected line, is identified as member of the PN. By applying a moving average filter on the identified dots, a 3D representation of the PN can be made. Figure 36 shows the result.

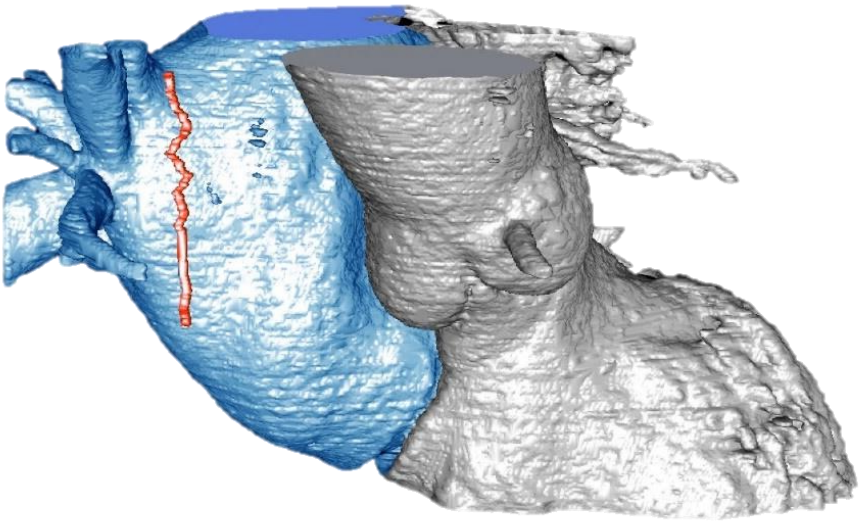

Figure 36: Reconstruction of the PN (red) with the segmented LA (blue) and aorta + left ventricle (grey)

5 Results and validation

The algorithm is tested on the CT slices of a series of 27 patients. First the segmentation step is reviewed. After that the results of the PN reconstruction algorithm are described. Finally, the location of the PN as identified by the physician is compared to the location found by the algorithm. For one test case, there is an additionally verification step, namely the comparison of the detected PN with the location of the PN defined by pace mapping.

5.1 Results of the segmentation step

The results of the segmentation are determined by manually reviewing each CT slice. The evaluation is based on the three main parts of the segmentation step:

- segmentation of the white contrast fluid (Attachment B)
- segmentation of the RA (Attachment C),
- determination of the nerve area (Attachment D).

For each of those three categories, the number of errors is calculated. These are all the slices where the detected part or region is too big, too narrow or not accurately located. Table 1, in Attachment F, gives an overview of the number of slices where the segmentation failed or succeeded and the accompanying accuracy results. A graphical presentation of this outcome is given in Graph 1. In this graph the accuracy rate is represented, this is the total number of correctly segmented slices divided by the total number of examined CT slices.

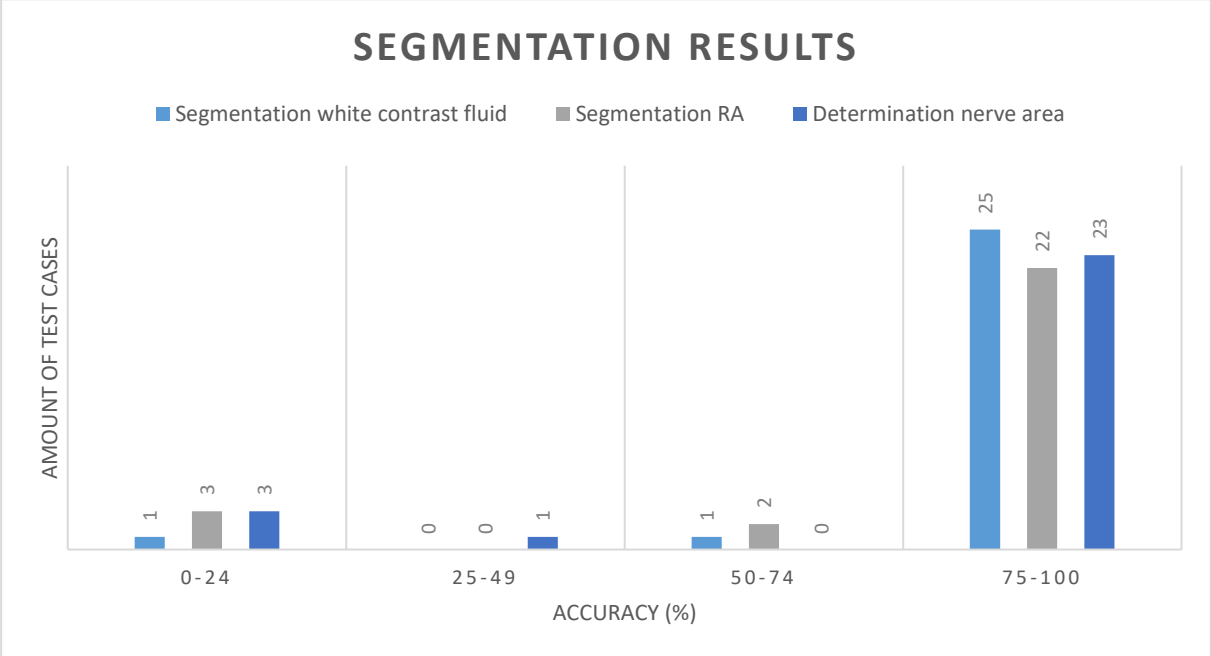

Graph 1: Segmentation results

Graph 1 is a histogram that divides the accuracy of the three segmentation methods in four groups. In 25 of the test cases the segmentation method of the white contrast fluid has an accuracy above 75 percent. Only in two cases, the segmentation method is not satisfying. For the other two methods, segmentation of the RA and determination of the nerve area, the same conclusions can be made. Respectively, five and four test cases do not meet an accuracy rate of 75 percent. In summary, the majority of the test cases has an accuracy between 75 and 100 percent of which 10 test cases have a success rate of 100 percent for the three methods.

5.2 Results of the PN reconstruction algorithm

The next step to evaluate is the PN reconstruction algorithm. The aim of this algorithm is to find the best fitting straight line in the 3D data point cloud. Sometimes, the detected line has a large range of x- and y-values. This means that the detected point moves a lot along the slices. Figure 37 illustrates some failed examples where all the detected PNs along the slices are indicated in red. In those cases, the PN detection will not succeed. This occurs mostly when the segmentation step has a low accuracy. This is the case for three of the 27 test patients. Therefore we can conclude that in 11 percent of the test cases, the algorithm will not work. For the other 89 percent of the cases, a plausible location of the PN can be found. The error margin of this detected point is calculated in the next section, the three test cases where the PN reconstruction algorithm failed (test cases nos. 13, 19, 22), are not taken into account.

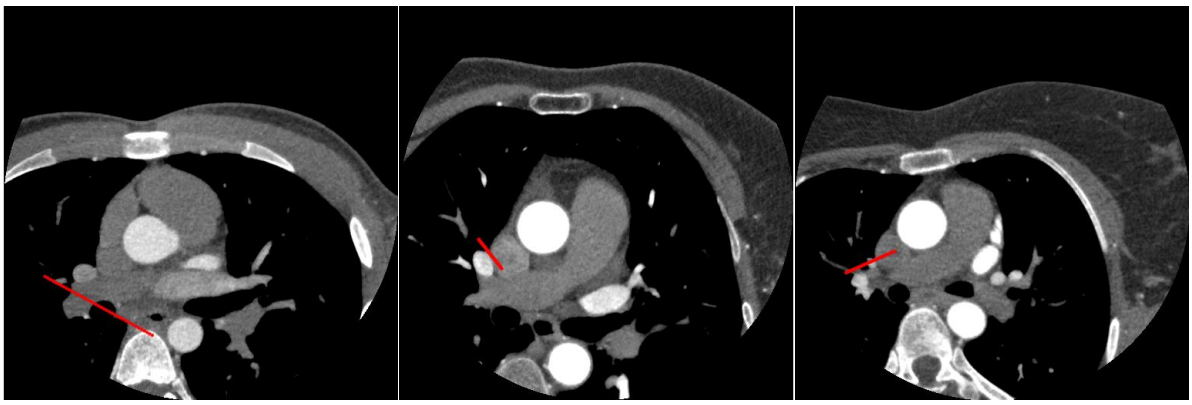

Figure 37: Failed detection

5.3 Results of the PN detection

To calculate the error margin of the algorithm, the distance between the PN determined by the algorithm (Attachment E) and the approximate location of the PN defined manually on the same CT slices by a trained electrophysiologist, is computed. For one test patient, validation is done by pace mapping the PN during surgery, which should be more accurate than 'eyeballing'.

Table 2, in Attachment G, shows the comparison between the location of the PN defined by the physician and the location found by the algorithm for the 24 test cases. The error margin shows the deviation between those locations. It can be concluded that the PN can be detected at the same spot as the physician claims it is located, with a median accuracy of 3.51mm. This is shown by the boxplot in Graph 2. In 75 percent of the test cases, the accuracy is better than 5.75 millimeters.

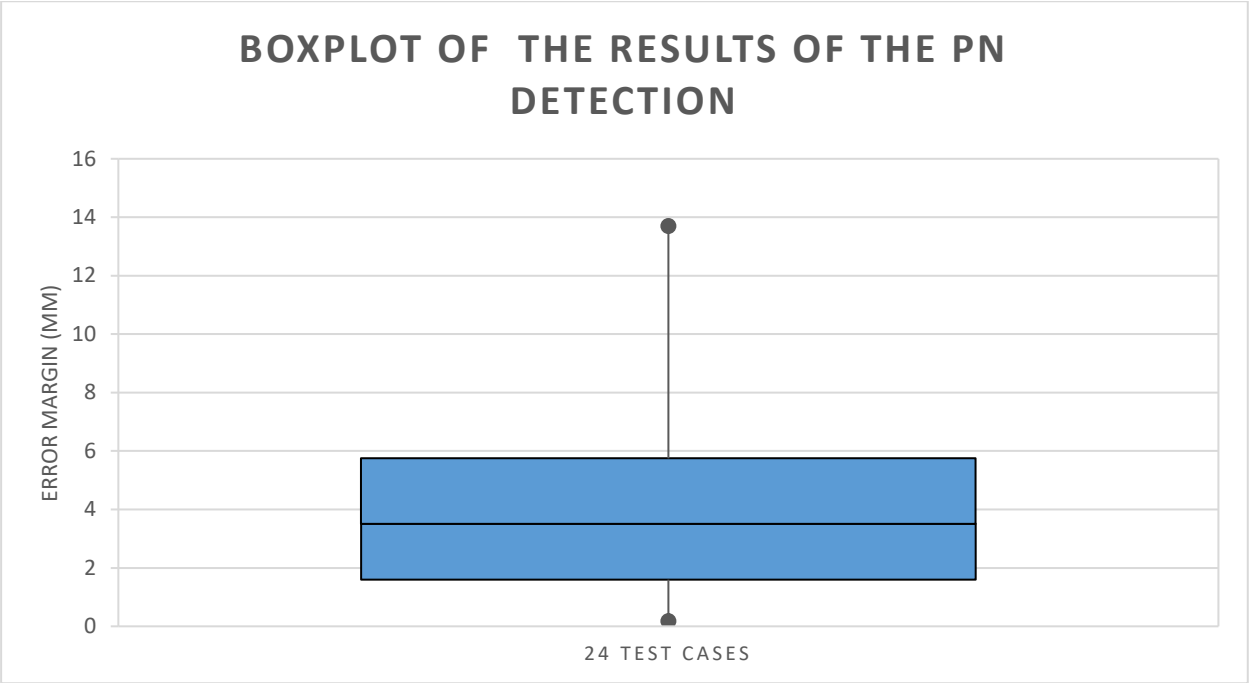

Graph 2: Boxplot of the error margins of the PN detection

Another representation of the error margins is given in Graph 3. In 10 out of the 24 test cases, the accuracy is better than 2.9 mm. The number of test cases decreases with higher error margin.

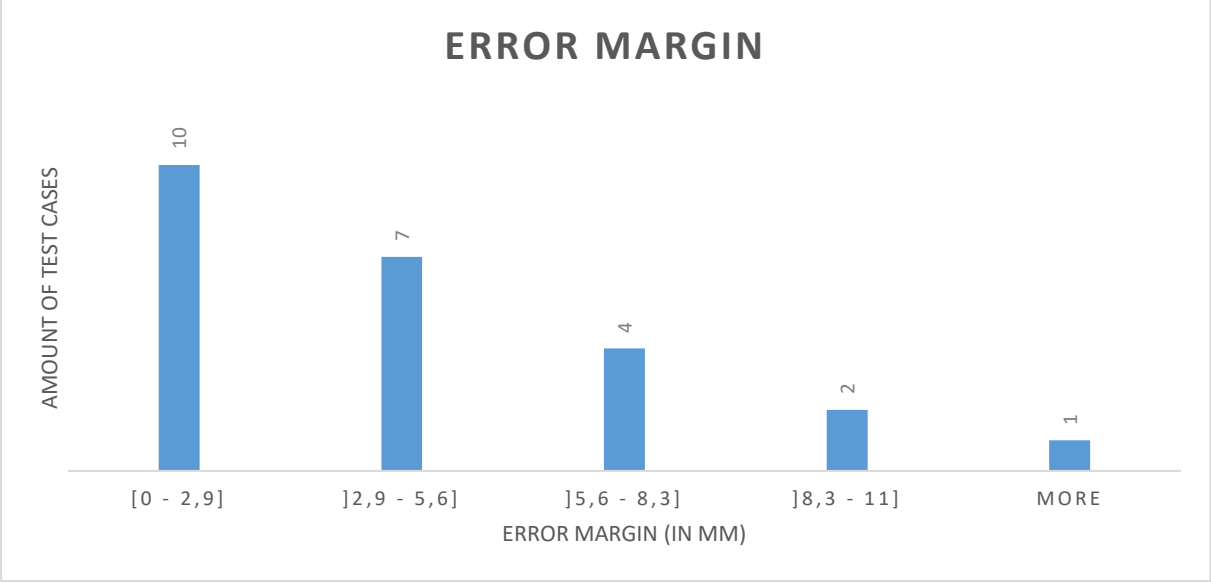

Graph 3: Histogram of the error margins

Additionally, validation is done by pacemapping for test case 27. Figure 38 is a representation of the model of the RA made during an electrophysiological procedure. The location of the PN is defined with a pacing catheter. At each point where the catheter stimulates the nerve, a green dot is placed. It should be noted that the location therefore is mapped on the surface of the RA and the distance between RA and PN cannot be derived from the model. Figure 39 is a representation of the segmented RA and detected PN by the algorithm. The green dots represent the detected PN locations, the orange line is the location of the nerve defined by the algorithm throughout the slices.

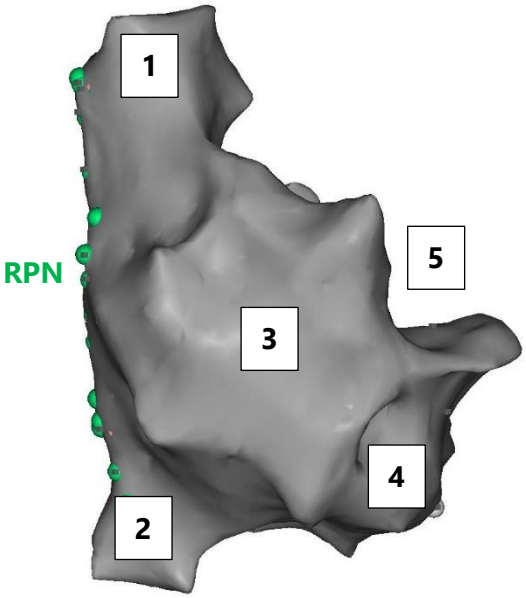

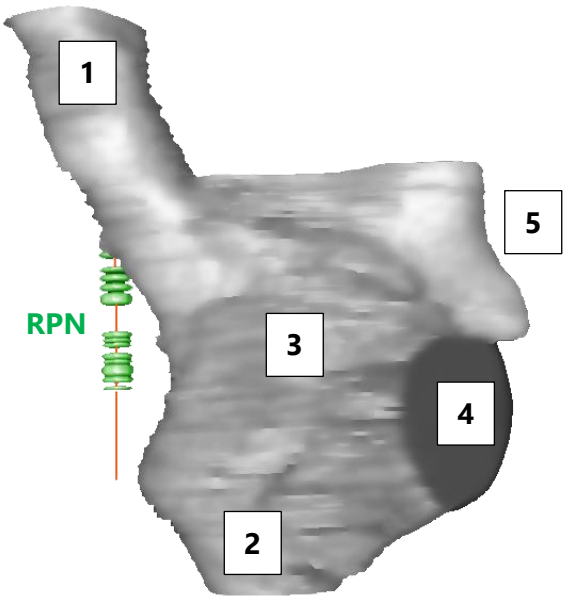

Model of the right atrium in RAO 38°

1: superior vena cava, 2: inferior vena cava, 3: right atrium, 4: tricuspid valve, 5: right atrial appendage

Figure 38: Model drawn up by pace mapping

Figure 39: Model drawn up by the algorithm

6 Discussion

Currently, the existing methods to detect and prevent damage to the right PN during pulmonary vein isolation are primitive and cumbersome. Visualizing the right PN could improve the workflow of the ablation procedure and reduce the likelihood of damaging the right PN. Our proposed algorithm can segment the different parts of the heart, namely the regions with contrast fluid (the aorta and the LA), the RA and the right ventricle. This part of the algorithm can also be used for other applications. To detect the PN, a likely 'nerve area' is defined based on this segmentation step. Our PN detection method has a success rate of 89 percent for all 27 test cases, examined in this research. It has a median accuracy value of 3.51 mm. In 24 cases the algorithm could predict a plausible location for the right PN, in contrast to the previous algorithm described in the bachelor's thesis, where detection on only one patient was successfully achieved. The current revised algorithm is able to perform the image processing calculations in on average 1.5 seconds per CT slice. The complexity of the execution time is of the order O(n), with n the amount of CT slices. This means that computing time increases proportionally with the number of CT slices to examine. The results open up new possibilities for further research. Furthermore, not much research has been done on this subject. As far as known by the authors, there are no other studies available about automatically detecting the right PN.

One of the limitations of this study is that the algorithm does not work for all of the test cases. The failure of the algorithm is mainly caused by the irregular anatomy of the heart. Another reason why the algorithm does not achieve 100 percent success rate is because of the contrast of the CT scan. The quality of the contrast depends on the size of the patient, the dose of injected contrast fluid and the radiology protocol of the CT images. Furthermore, the zoom percentage of the CT scan is a crucial factor for the algorithm to succeed. Another limitation is that the detected PN is a straight line, but in fact the nerve bends a little bit. By adapting the PN reconstruction algorithm for the identification of a polynomial, the accuracy of the PN detection could be enhanced.

To evaluate the results, the right PN is visually determined by a trained electrophysiologist on one CT slice for each patient. These locations are not totally reliable because the physician is not able to detect the right PNs accurately for all patients. However, the error margin gives an approximation of the accuracy of the algorithm in comparison with manual detection. Another approach is to use pace mapping to indicate the location of the phrenic nerve more accurately. In the 3D mapping software provided in the CATHLAB (CARTO ® 3, Biosense Webster, Diamond Bar, California), a visualization of the right atrium with the pace mapped PN can be made. This model indicates the location of the PN, projected on the RA. The exact distance between the pace mapped PN and the reconstructed nerve cannot be measured, but the visualization gives an idea of the accuracy of the algorithm. A side note is that the pace mapping technique has a measuring accuracy of only 0.5 to 1 centimeter. The median accuracy value of 3.51 mm of our algorithm seems to be higher.

The segmentation methods are only tested on high resolution CT slices. Most probably, the results will be less successful for a CT scan of lower quality. The final purpose of this study is to detect the right PN on a 3D rotational angiography. To achieve this, a possible methodology

would be to split up this 3D model in slices similar to CT slices. Probably low resolution issues will have to be dealt with.

7 Conclusion

The visualization of the right PN is important to prevent paralysis. In this research an algorithm is developed to indicate the PN on high resolution CT slices. By segmentation of the different parts of the heart, a 'nerve area' can be defined where possible PN locations can be found. The last step is 3D reconstruction of the nerve by using the developed variant of the RANSAC method, the "PN reconstruction algorithm". In 89 percent of the 27 test cases, the PN detection was successful. The plausible PN location has a median accuracy value of 3.51 mm. It should be noted that there is an error margin on the PN locations indicated by the physician because the PN is not always clearly visible on CT scans. To conclude, this thesis is a major step forward to the ultimate goal of this study, identification of the PN on 3D rotational angiography.

References

[1] K. Bamps and P. Polmans, "Automatic identification and reconstruction of the right phrenic nerve on computed tomography – proof of concept," pp. 1–8, 2016.

[2] Mathworks, "MathWorks - Makers of MATLAB and Simulink." [Online]. Available: https://nl.mathworks.com/. [Accessed: 06-Apr-2017].

[3] Hamilton Cardiology Associates, "Atrial Fibrillation – Hamilton Cardiology Associates – New Jersey's Leading Board Certified Cardiologists." [Online]. Available: https://www.hcahamilton.com/atrial-fibrillation. [Accessed: 24-May-2017].

[4] Osmosis, *Atrial fibrillation (A-fib, AF) - causes, symptoms, treatment & pathology*. 2016.

[5] StopAfib.org, "Atrial Fibrillation Catheter Ablation Technology—Balloon Catheters," 2012. [Online]. Available: http://www.stopafib.org/catheter-ablation/technology-balloon.cfm. [Accessed: 05-Apr-2017].

[6] G.-B. CHIERCHIA *et al.*, "Impact on Clinical Outcome of Premature Interruption of Cryoenergy Delivery Due to Phrenic Nerve Palsy During Second Generation Cryoballoon Ablation for Paroxysmal Atrial Fibrillation," *J. Cardiovasc. Electrophysiol.*, vol. 26, no. 9, pp. 950–955, Sep. 2015.

[7] S. R. Dukkipati *et al.*, "Pulmonary Vein Isolation Using a Visually Guided Laser Balloon Catheter: The First 200-Patient Multicenter Clinical Experience," *Circ. Arrhythmia Electrophysiol.*, vol. 6, no. 3, pp. 467–472, Jun. 2013.

[8] prof. dr. J. W. S. prof. dr. J.B.M. Kuks, *Klinische Neurologie*. 2012.

[9] S. L. Aquino, G. R. Duncan, and A. L. Hayman, "Nerves of the Thorax: Atlas of Normal and Pathologic Findings," *RadioGraphics*, vol. 21, pp. 1275–1281, 2001.

[10] B. Schmidt, K. R. J. Chun, F. Ouyang, A. Metzner, M. Antz, and K.-H. Kuck, "Three-dimensional reconstruction of the anatomic course of the right phrenic nerve in humans by pace mapping," *Hear. Rhythm*, vol. 5, no. 8, pp. 1120–1126, 2008.

[11] R. Horton *et al.*, "Locating the right phrenic nerve by imaging the right pericardiophrenic artery with computerized tomographic angiography: Implications for balloon-based procedures," *Hear. Rhythm*, vol. 7, no. 7, pp. 937–941, 2010.

[12] R. C. Gonzalez, Rafael C. Gonzalez, Richard E.Woods, and S. L. Eddins, "Digital image processing using matlab," *Ceit.Aut.Ac.Ir*. p. 609, 2009.

[13] MathWorks, "Edge Detection - MATLAB & Simulink." [Online]. Available: https://nl.mathworks.com/discovery/edge-detection.html. [Accessed: 07-Apr-2017].

[14] R. Schnabel, R. Wahl, and R. Klein, "Efficient RANSAC for Point-Cloud Shape Detection," *Comput. Graph. Forum*, vol. 26, no. 2, pp. 214–226, Jun. 2007.

[15] J. D. Foley, M. A. Fischler, and R. C. Bolles, "Graphics and Image Processing Random Sample Consensus: A Paradigm for Model Fitting with Apphcatlons to Image Analysis and Automated Cartography."

[16] NEMA, "Digital Imaging and Communications in Medicine." [Online]. Available: http://dicom.nema.org/. [Accessed: 07-Apr-2017].

[17] D. R. Varma, “Managing DICOM images: Tips and tricks for the radiologist.,” *Indian J. Radiol. Imaging*, vol. 22, no. 1, pp. 4–13, Jan. 2012.

[18] MathWorks, “Read DICOM image - MATLAB dicomread - MathWorks Benelux.” [Online]. Available: https://nl.mathworks.com/help/images/ref/dicomread.html. [Accessed: 06-Apr-2017].

[19] B. (Philips) Revet, “DICOM Cook Book for Implementations in Modalities,” vol. 14, 1997.

[20] R. Kumar, “Diffusion Filtering for Image Denoising - File Exchange - MATLAB Central,” 2010. [Online]. Available: http://nl.mathworks.com/matlabcentral/fileexchange/28112-diffusion-filtering-for-image-denoising?focused=5167065&tab=function. [Accessed: 12-May-2017].

[21] Eli Billauer, “peakdet: Peak detection using MATLAB,” 2012. [Online]. Available: http://billauer.co.il/peakdet.html. [Accessed: 24-Mar-2017].

Attachments

Attachment A: PN reconstruction algorithm

```
Given:

        t - Threshold that determines when a point fits to the line.

        data - The 3D point cloud of candidates for PN-location (XYZ). This is a colomn vector
        with as rows XYZ.

        s1 - Amount of slices taken into account starting from the top

        s2 - Amount of slices taken into account starting from the bottom

Return:

        line - The best fitting line

        inliers - Amount of inliers

        bestRatio - The ratio between the number of inliers and the length of the line


bestRatio = 0

L = []


for every point that lies in the interval between the first z-value and the z-value + s1 {

        for every point that lies in the interval between the last z-value and the z-value - s2 {

                maybeLine = a line between a point in the top and in the bottom of the data

                numberOfInliers = 0

                for every point in the data {

                        if the point fits the maybeLine with an error lower than t {

                                numberOfInliers++

                        }

                }


                if the numberOfInliers/length of the line is greater than bestRatio {

                        line =  start and end point of the maybeLine

                        inliers = amount of inliers

                        bestRatio = numberOfInliers/length

                }

        }

}
```

Attachment B: Detection of the white contrast fluid

Figure 40 shows the detected regions with white contrast fluid for test case 1. The range of the CT slices goes from 30 to 180, with steps of 5 slices. The range is selected based on the slice where the upper pulmonary vein connects to the LA and the slice where the lower pulmonary vein is not visible anymore.

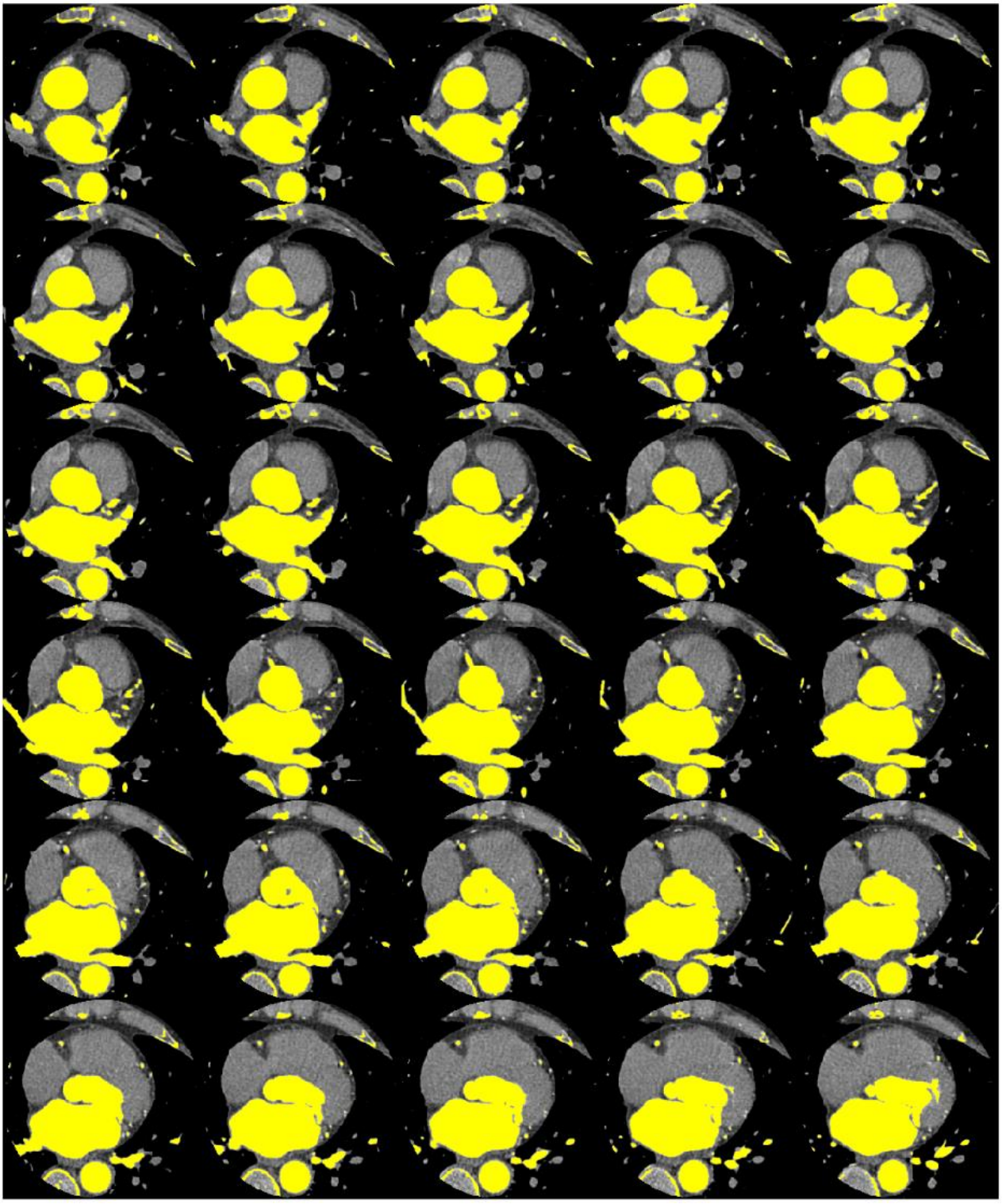

Figure 40: Detection of the white contrast fluid

Attachment C: Detection of the right atrium and right ventricle

Figure 41 shows the detected right atrium and right ventricle for test case 1 (CT slices 30-180).

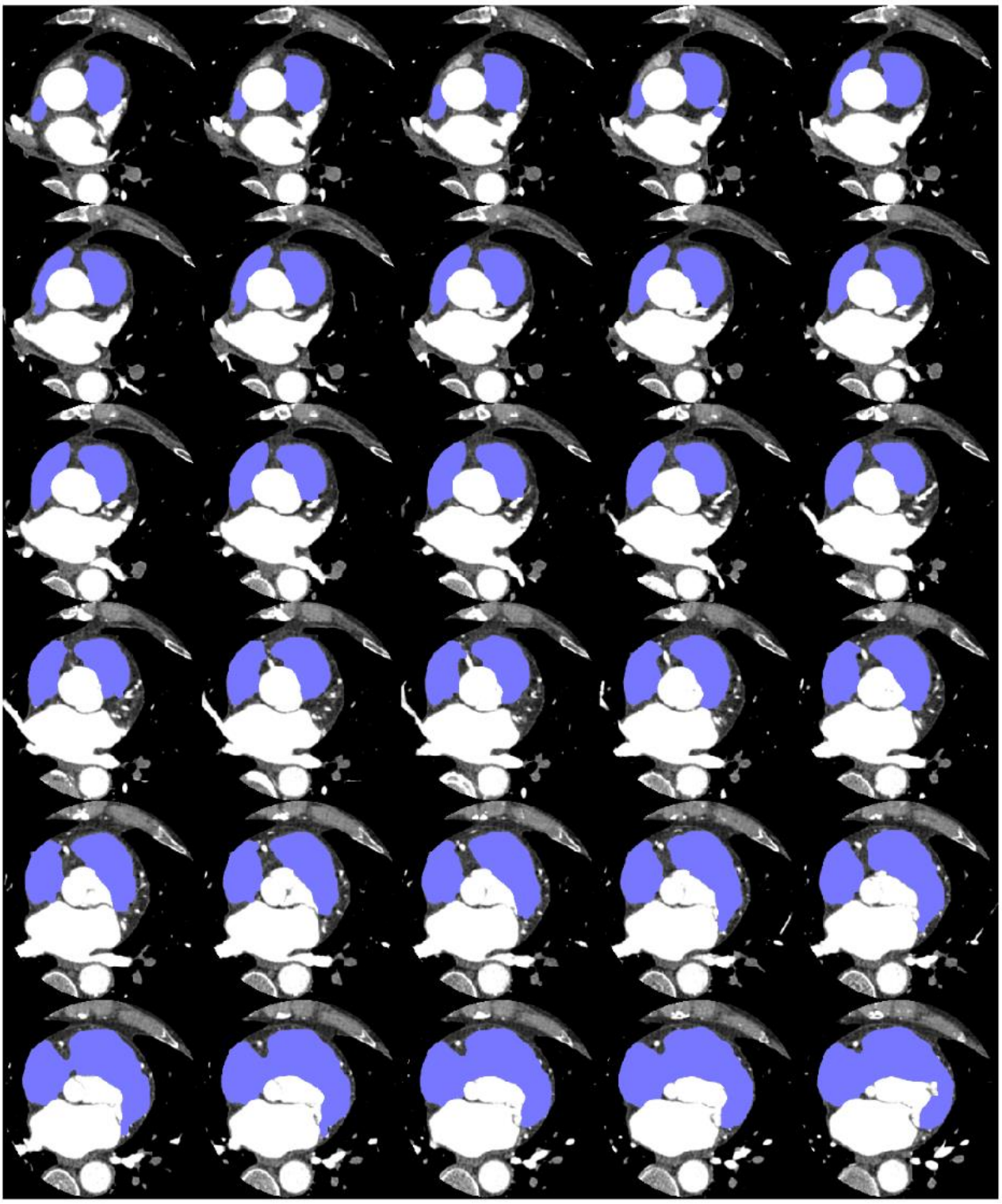

Figure 41: Detection of the RA

Attachment D: Determination of the nerve area

The algorithm determines a nerve area by using the segmented areas with white contrast fluid (indicated in yellow) and the right atrium (indicated in blue). Figure 42 indicates this region in orange for test case 1 (CT slices 30–180).

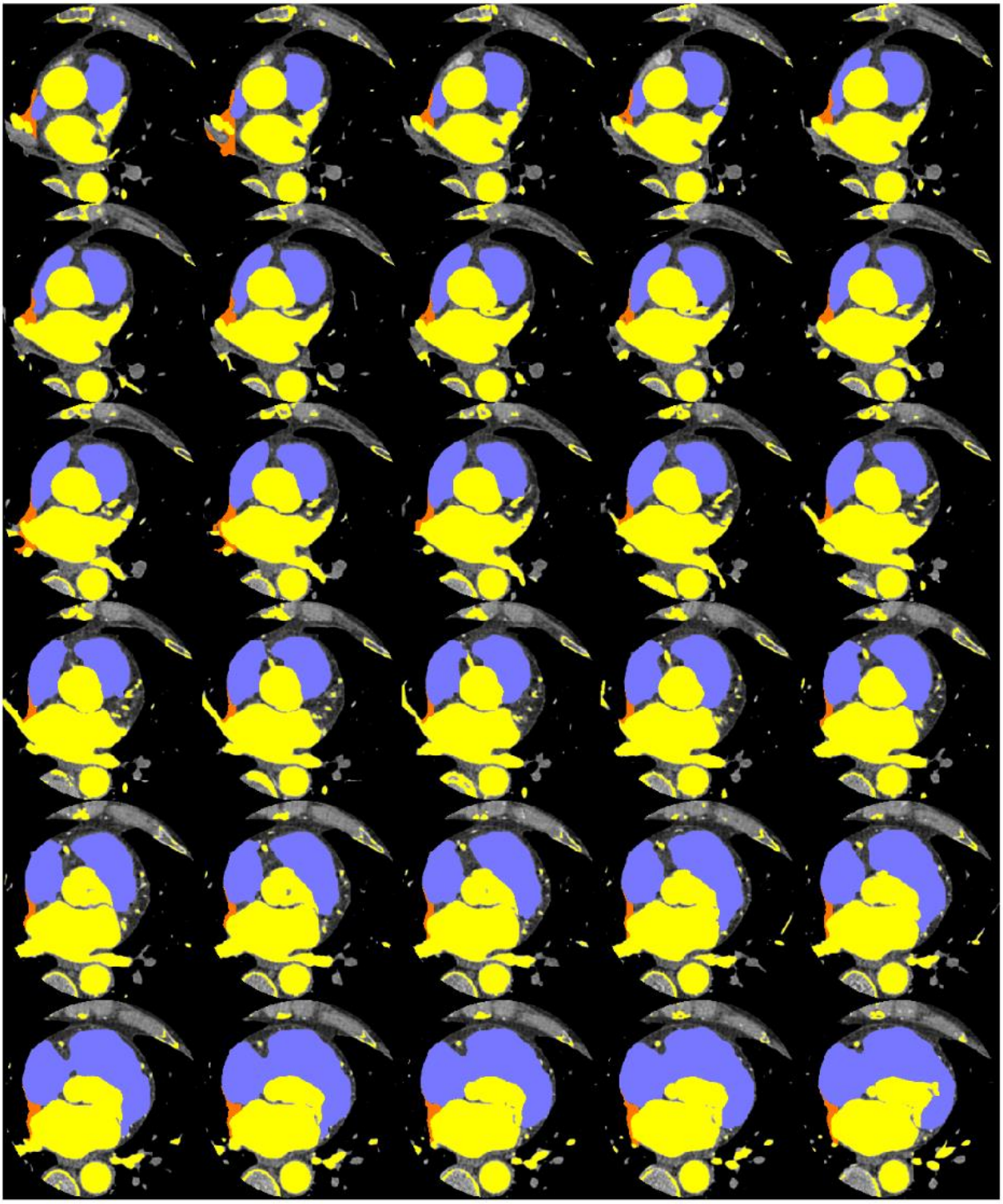

Figure 42: Determination of the nerve area

Attachment E: Detection of the PN

In Figure 43, the PN location defined by the algorithm for test case 1 (CT slices 30-180) is indicated with a green circle.

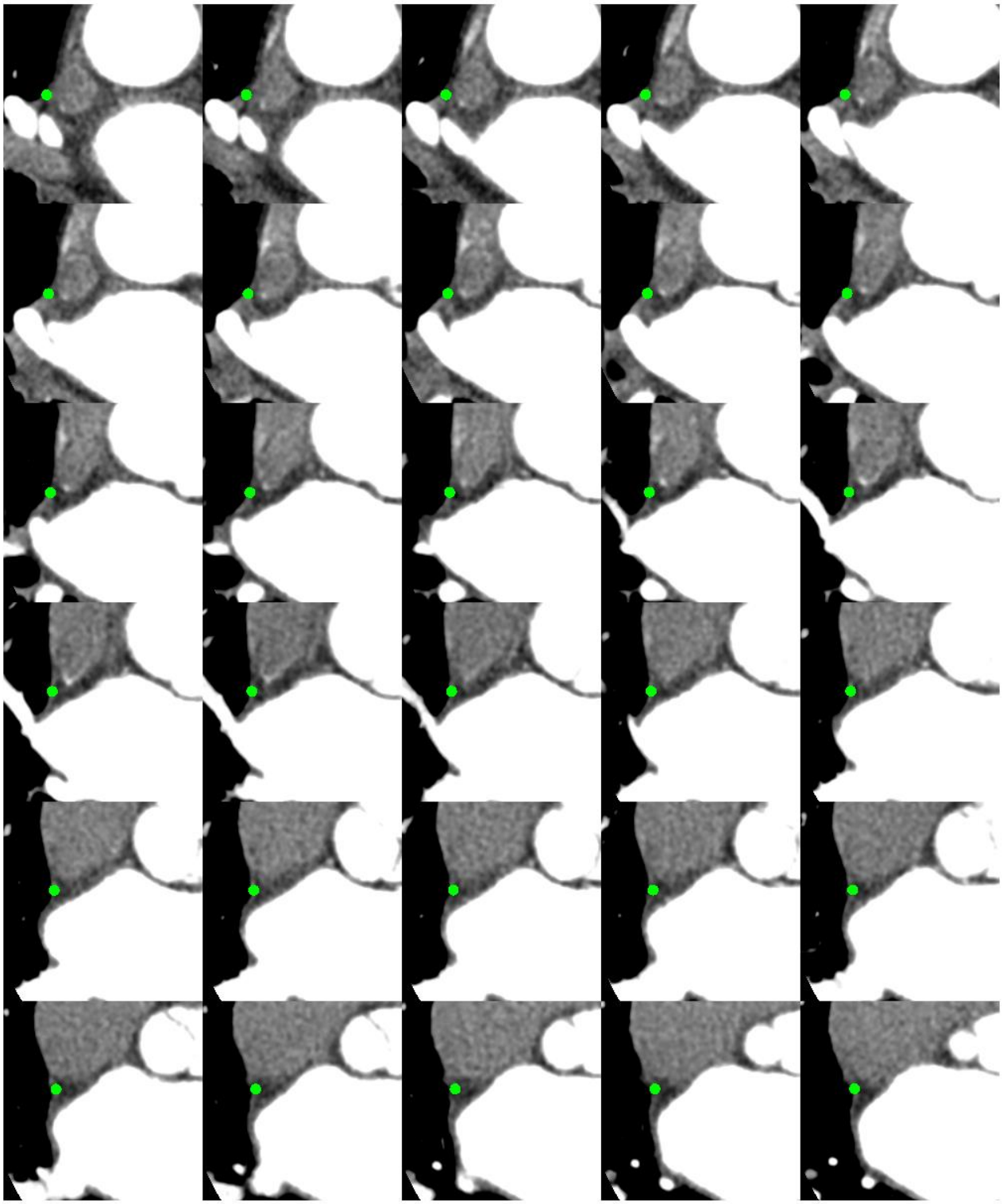

Figure 43: Detection of the PN

Attachment F: Overview of the segmentation results

Table 1 shows the segmentation results of the 27 test cases. The column 'errors' represents the number of slices that were not correctly segmented by the given method. The accuracy is computed by dividing the correctly segmented slices by the total number of slices.

		ERRORS			ACCURACY		
	Number of slices	Segmentation white contrast fluid	Segmentation right atrium	Determination nerve area	Segmentation white contrast fluid	Segmentation right atrium	Determination nerve area
Test case 1	150	0	0	0	100.00	100.00	100.00
Test case 2	178	0	2	0	100.00	98.88	100.00
Test case 3	154	0	0	94	100.00	100.00	38.96
Test case 4	110	4	0	0	96.36	100.00	100.00
Test case 5	110	0	0	0	100.00	100.00	100.00
Test case 6	145	3	0	0	97.93	100.00	100.00
Test case 7	130	2	52	0	98.46	60.00	100.00
Test case 8	130	2	2	0	98.46	98.46	100.00
Test case 9	100	0	0	0	100.00	100.00	100.00
Test case 10	70	0	11	0	100.00	84.29	100.00
Test case 11	66	1	1	8	98.48	98.48	87.88
Test case 12	66	0	2	1	100.00	96.97	98.48
Test case 13	60	0	0	0	100.00	100.00	100.00
Test case 14	100	0	0	0	100.00	100.00	100.00
Test case 15	110	0	0	11	100.00	100.00	90.00
Test case 16	105	0	0	0	100.00	100.00	100.00
Test case 17	110	0	0	3	100.00	100.00	97.27
Test case 18	40	32	32	40	20.00	20.00	0.00
Test case 19	40	0	37	37	100.00	7.50	7.50
Test case 20	70	2	2	0	97.14	97.14	100.00
Test case 21	130	0	4	0	100.00	96.92	100.00
Test case 22	40	0	39	32	100.00	2.50	20.00
Test case 23	40	0	0	0	100.00	100.00	100.00
Test case 24	145	0	0	0	100.00	100.00	100.00
Test case 25	50	0	0	0	100.00	100.00	100.00
Test case 26	70	25	25	0	64.29	64.29	100.00
Test case 27	70	0	0	0	100.00	100.00	100.00

Table 1: Errors and accuracy of the segmentation step

Attachment G: Error margins of the PN detections

Table 2 shows the error margin for each test case. This is the distance between the location of the PN defined by the physician and the location determined by the algorithm. The physician has indicated the nerve on one slice for every test case. The test cases on which the PN reconstruction algorithm fails, are not taken into account.

		Detected manually		Detected by the algorithm		Error margin	
	Slice	**X**	**Y**	**X**	**Y**	**in pixels**	**in mm**
Test case 1	78	68	278	67.95	279.6	1.60	0.54
Test case 2	58	67	324	69.63	342	18.19	6.13
Test case 3	211	42	283	51.88	273.6	13.64	4.60
Test case 4	350	98	372	112.5	381.5	17.33	5.84
Test case 5	209	67	290	70.31	281.1	9.50	3.20
Test case 6	160	91	266	93.71	264.4	3.15	1.06
Test case 7	189	111	302	110.6	307.3	5.32	1.79
Test case 8	227	75	307	76.08	292.9	14.14	4.77
Test case 9	150	70	310	71.39	305.1	5.09	1.72
Test case 10	195	108	340	118	342.1	10.22	3.44
Test case 11	113	58	337	65.97	336.2	8.01	2.70
Test case 12	87	54	310	64.37	313	10.80	3.64
Test case 13	Detection failed						
Test case 14	175	101	327	103.3	326.6	2.33	0.79
Test case 15	180	74	275	74.5	276.2	1.30	0.44
Test case 16	194	101	322	114.9	347	28.60	9.64
Test case 17	205	73	270	74.93	276.51	6.79	2.29
Test case 18	125	105	300	117.3	333.5	35.69	12.03
Test case 19	Detection failed						
Test case 20	63	108	335	120.71	345.73	16.63	5.61
Test case 21	153	103	326	100	320.4	6.35	2.14
Test case 22	Detection failed						
Test case 23	98	105	276	113.9	297.5	23.27	7.84
Test case 24	110	110	298	113.2	306.3	8.90	3.00
Test case 25	61	103	282	111.4	293.4	14.16	4.77
Test case 26	98	118	346	111.2	322.3	24.66	8.31
Test case 27	147	86	327	91.17	333.5	8.31	2.80

Table 2: Error margins PN detection

Auteursrechtelijke overeenkomst

Ik/wij verlenen het wereldwijde auteursrecht voor de ingediende eindverhandeling:
Automatic identification and reconstruction of the right phrenic nerve on computed tomography

Richting: **master in de industriële wetenschappen: elektronica-ICT**
Jaar: **2017**

in alle mogelijke mediaformaten, - bestaande en in de toekomst te ontwikkelen - , aan de Universiteit Hasselt.

Niet tegenstaand deze toekenning van het auteursrecht aan de Universiteit Hasselt behoud ik als auteur het recht om de eindverhandeling, - in zijn geheel of gedeeltelijk -, vrij te reproduceren, (her)publiceren of distribueren zonder de toelating te moeten verkrijgen van de Universiteit Hasselt.

Ik bevestig dat de eindverhandeling mijn origineel werk is, en dat ik het recht heb om de rechten te verlenen die in deze overeenkomst worden beschreven. Ik verklaar tevens dat de eindverhandeling, naar mijn weten, het auteursrecht van anderen niet overtreedt.

Ik verklaar tevens dat ik voor het materiaal in de eindverhandeling dat beschermd wordt door het auteursrecht, de nodige toelatingen heb verkregen zodat ik deze ook aan de Universiteit Hasselt kan overdragen en dat dit duidelijk in de tekst en inhoud van de eindverhandeling werd genotificeerd.

Universiteit Hasselt zal mij als auteur(s) van de eindverhandeling identificeren en zal geen wijzigingen aanbrengen aan de eindverhandeling, uitgezonderd deze toegelaten door deze overeenkomst.

Voor akkoord,

Bamps, Kobe **Cuypers, Céline**

Datum: **5/06/2017**